WAPD-T-3173

THE CORROSION OF ZIRCALOY-CLAD FUEL ASSEMBLIES IN A GEOLOGIC REPOSITORY ENVIRONMENT

E. Hillner
D. G. Franklin
J. D. Smee

Contract No. DE-AC11-93PN38195

NOTE

BETTIS ATOMIC POWER LABORATORY WEST MIFFLIN, PENNSYLVANIA 15122-0079

Operated for the U.S. Department of Energy
by WESTINGHOUSE ELECTRIC CORPORATION

THE CORROSION OF ZIRCALOY-CLAD FUEL ASSEMBLIES IN A GEOLOGIC REPOSITORY ENVIRONMENT

E. Hillner, D.G. Franklin, and J.D. Smee

ABSTRACT

Recently analyzed long-term Zircaloy autoclave corrosion data were used to develop new Zircaloy corrosion correlations. Calculations were performed to estimate the additional quantity of corrosion that may be experienced by spent Zircaloy-clad fuel assemblies from long-term exposure to geologic repository conditions. These estimates indicate that the level of general corrosion is very small and will not be expected to affect the integrity of nonfailed fuel elements with Zircaloy-4 cladding through the life of a repository.

Twenty-two different autoclave tests were analyzed. The tests included specimens from 46 different heats, of both Zircaloy-2 and Zircaloy-4. The material conditions included different heat treatments and various prefilms. Maximum exposure time was 10,507 days (~29 years) in a 600°F (316°C) test and maximum weight gain was 1,665 mg/dm^2 (~4.5 mils of oxide film) for a 640°F (338°C) experiment. The new kinetic data, with various conservative assumptions, were used in conjunction with a projected fuel temperature profile during disposal to generate a best-estimate prediction of ~0.3 mils of additional oxide film growth after one million years exposure in the repository. This additional oxide film growth should not pose a threat to the integrity of the Zircaloy cladding. A review of the fundamental factors affecting corrosion indicates that the extrapolation from the test database to repository times is reasonable, in part because the database covers the thickness of oxides expected for repository disposal. It also is shown that the ionic constituents of typical ground water, in the anticipated concentrations and pH levels, will have no discernible detrimental effect on the corrosion behavior of Zircaloy in the repository environment.

BACKGROUND

The safe repository disposal of spent fuel elements is important for the nuclear power industry because it closes the nuclear fuel cycle. Currently, expended fuel assemblies are being stored, temporarily, in water pools or in above-ground dry facilities at the various power plants. The US Department of Energy (DOE) has been given the task of establishing long-term disposal capability for spent fuel, which will allow utilities to continue operations and close plants at the scheduled end of life.

Expended cores from naval nuclear reactors are stored in water pools, with dry storage capability being planned. Disposal will be in the same national repository being developed for commercial fuel. Therefore, the Naval Reactors program is performing testing and analyses to demonstrate that naval expended cores can be disposed of safely in the national geologic repository. The primary function of the repository is to protect the environment by delaying and controlling the release of radioactive material into the environment. Although the disposal canisters and the ground provide the barriers to the release of materials, Zircaloy fuel cladding provides a significant additional barrier. This report evaluates whether the integrity of the cladding surrounding spent fuel elements to be interred in the repository will be compromised during the prolonged

exposure to the repository surroundings via a corrosion-related mechanism. Cladding integrity is important since the cladding is the final barrier between the irradiated fuel and the repository environment, regardless of the final containment design. Of all properties relevant to the entire wastage package i.e., both the spent fuel assemblies and the repository containment materials, the most important is corrosion. The anticipated cladding corrosion in the repository could also be factored into the analysis of potential criticality in the repository and the choice of materials for the outer containment barriers.

To date, the fuel-element cladding of choice for most nuclear power plants has been one of two Zircaloys, which are alloys of zirconium with small amounts of tin, iron, and chromium as alloying additions. Zircaloy-4 is used in both pressurized water reactors (PWR) and boiling water reactors (BWR). Zircaloy-2, which is used extensively in BWRs, also has small amounts of nickel as an alloying addition. The two properties of zirconium alloys that largely influenced their selection for cladding are their excellent high-temperature water-corrosion resistance and very low thermal neutron absorption cross-section. Since these two Zircaloys exhibit similar corrosion behavior at repository conditions, only the generic term "Zircaloy" will be employed in this report. However, all discussions and conclusions in this document apply to both Zircaloy-2 and Zircaloy-4.

AQUEOUS CORROSION OF ZIRCALOY

Introduction

The database most appropriate to establish a basis for Zircaloy corrosion behavior in a repository environment is isothermal aqueous autoclave corrosion data. Under present considerations it is anticipated that when the final barrier in the repository is breached, and ground water can come in contact with the Zircaloy-clad spent fuel elements, the vast majority of additional repository exposure would take place at temperatures in the neighborhood of ~200°F (~93°C) and below. The preponderance of Zircaloy autoclave data have been generated in the temperature range 480°F to 680°F (250°C to 360°C) in degassed, deionized water and with relatively short exposure times for the lower exposure temperatures. The excellent corrosion resistance of Zircaloy makes it impractical to conduct meaningful testing below ~450°F (230°C) in any reasonable time period. Thus, it will be necessary to employ corrosion models based on data generated at the higher temperatures and extrapolations have to be made to the lower temperatures anticipated in the repository.

Model Development

Zircaloy reacts with water to form a corrosion film of ZrO_2, by the following reaction:

$$Zr + 2H_2O \rightarrow ZrO_2 + 2H_2 \qquad [1]$$

Since virtually all of the oxygen generated in Equation [1] reacts with the Zircaloy to form the corrosion film and the film remains adherent, the weight gain of the corrosion specimens has been used as a direct gauge of the oxide film thickness[1]. The Zircaloy corrosion processes are known to occur in three stages:

---

[1]378 mg/dm^2 of weight gain = 1 mil of oxide growth = 0.66 mils of metal consumed.

1. The early pretransition regime, characterized by the formation of a thin, black, tightly adherent corrosion film that grows thicker in accordance with a cubic rate law,

2. The midlife transition, or transitory stage, that lies between the pretransition and posttransition stages. As initially shown by Bryner [REFERENCE 1], this region appears to be comprised of a series of successive cubic curves, similar to the initial cubic kinetic curve, but initiating at shorter and shorter intervals, and

3. The linear posttransition kinetic regime.

The three-stage Zircaloy corrosion behavior is shown schematically in Figure 1. The dashed lines in Figure 1 indicate that most early corrosion models recognized only the pretransition and posttransition kinetic regimes. Since some spent naval fuel cladding will be in the posttransition region upon entry into the repository, i.e., oxide film thicknesses in excess of 1 mil, this document will be concerned only with posttransition corrosion behavior. The use of these kinetics will be conservative for cladding that may not have attained the posttransition region prior to disposal.

Posttransition corrosion kinetics can be described by an expression of the form:

$$\Delta W = K_L t + C \qquad [2]$$

where

ΔW = specimen weight gain, in units of mg/dm^2,
t = exposure time, in units of days,
K_L = empirical constant, usually termed the linear (or posttransition) rate constant, in units of $mg/dm^2/day$, and
C = another constant, in the same units as ΔW (mg/dm^2), which is the intercept of the linear equation at zero time.

From Equation [2], a plot of the weight gain as a function of the exposure time produces a straight line with a slope equal to K_L and an intercept equal to the constant, C. The temperature dependence of the linear rate constant (K_L) has been shown to follow an Arrhenius-type behavior of the form:

$$K_L = B \exp[-Q_L/RT] \qquad [3]$$

where:

B = an empirical constant, in units of $mg/dm^2/day$,
Q_L = the activation energy for the posttransition (linear) corrosion region, in units of cal/mol,
R = universal gas constant, 1.98 cal/mol-°K, and
T = absolute temperature, in units of °K.

Thus, from Equation [3], a plot of the natural logarithm of the linear rate constant [$Ln(K_L)$] against the reciprocal of the absolute temperature generates a straight line with a slope equal to $-Q_L/R$ and an intercept on the Y axis equal to the natural logarithm of the constant, B. Combining Equations [2] and [3] results in the following general expression for the posttransition corrosion of Zircaloy as a function of both time and temperature:

$$\Delta W = (B \exp[-Q_L/RT] \times t) + C. \quad [4]$$

Many isothermal autoclave corrosion studies of the Zircaloys have been conducted, primarily in the temperature range of 550°F to 750°F (~290°C to 400°C) [REFERENCES 2 - 19]. In 1976 Hillner [REFERENCE 11] compiled the data from REFERENCES 2 - 10 into engineering curves for each exposure temperature and, generating an activation energy for the posttransition rate constant, K_L, produced the following empirical expression for posttransition behavior:

$$\Delta W = 1.12 \times 10^8 \exp[-12{,}529/T] \times t \quad [5]$$

where all of the terms have been defined previously. During analyses of the Zircaloy corrosion data, the constant C was found to be small and not included in Equation [5]. (Note that for ease of calculation the parameter Q_L/R has been combined into a single value in the above equation).

Several additional Zircaloy corrosion models have been published in the technical literature [REFERENCES 12 - 19]. Most models follow the form of Equation [4] for posttransition behavior and those that do not can be converted easily to this format. For the current application it is of interest to compare predictions from the various models for prolonged exposure to a low-temperature environment. Rothman [REFERENCE 20] has proposed an assumption of a constant temperature of 356°F (180°C) for 10,000 years as a possible spent fuel disposal scenario for a compacted-volcanic-ash (tuff) repository. Using Rothman's exposure conditions, calculations were conducted with eight different corrosion correlations to determine the anticipated extent of additional Zircaloy corrosion, assuming that the fuel cladding was in the posttransition kinetic regime upon disposal. Table 1 shows the results of such calculations. The prediction for the REFERENCE 11 model was based on the use of Equation [5], above.

All of the numbers in Table 1 have been rounded. The predicted extent of corrosion for all of the models shown in Table 1 reflect the excellent corrosion resistance of Zircaloy, for these assumed conditions for tuff repository disposal.

Comparisons with Equation [5] have been conducted in many investigations [REFERENCES 15-18, 20-30]. Almost all of these early models suffer from one major weakness when repository predictions are concerned; in general, there is a paucity of data for extended exposures in the posttransition region, especially at low temperatures. The Bettis Atomic Power Laboratory has generated a considerable quantity of autoclave corrosion data since the publication of REFERENCE 11. The sections below present these new data, discuss the generation of new posttransition corrosion equations, and assess the impact of these equations on the long-term repository oxide-film growth predictions.

New Corrosion Test Data

1. Test Description

The tests were conducted in static isothermal autoclaves at temperatures of 520°F to 680°F (271°C to 360°C). Specimen dimensions were typically 1 inch (25 mm) by 1 inch by ~0.060 inch (1.5 mm) to 0.100 inch (2.5 mm) thick. Periodic weight measurements were obtained during exposure in twenty-two different autoclave tests. These specimens represented a total of 46

Zircaloy-2 and Zircaloy-4 heats with different heat treatments and with various prefilms. The number of specimens in each test decreased with increasing exposure since coupons were removed periodically for destructive analyses. For this repository disposal application, long-term exposure data are of the most interest. Therefore, this analysis concentrated only on the post-transition kinetic region. It was assumed that weight gains of approximately 45 mg/dm^2 and above were in posttransition[2] and the weight changes were tabulated from this point on. Maximum exposure time for any specimen was 10,507 days (~29 years) in a 600°F (316°C) test (test #5) and the maximum weight gain was 1,665 mg/dm^2 (~4.5 mils or ~ 114 μm of oxide) in a 640°F (338°C) experiment (test #12).

2. Test Data

Table 2 provides a summary of the material and test conditions employed in these tests.

For groups of coupons that are nominally identical and tested together in the same autoclave in each test, specimen weight gains were averaged for each exposure time and the average weight (mg/dm^2) plotted as a function of total exposure time (days). This averaging was done to prevent domination of the analysis by times or temperatures at which many data were collected. Appendix A describes how the SOLO statistical software package was used to handle the raw data and to generate the algorithms that show the best fit with the weight gain versus time data.

Figure 2A shows a typical data plot at 680°F (360°C) from test #21. The solid line in this plot is the least-squares straight line drawn through all of the posttransition data. The curvature of the data about this line is readily apparent and cannot be ignored. Thus, the posttransition kinetic region can no longer best be described by a single posttransition rate constant, like that shown in Equations [2] and [3]. Using the SOLO statistical program, it was found that a series of two successive linear equations, each active over a different time range, best describe the data. Figure 2B is a replot of the data of Figure 2A showing the two linear rate constants. For purposes of discussion the early linear portion has been designated as stage 1 and the later linear behavior has been called stage 2. The software package automatically calculates both the time and weight gain at the transition point between the two linear stages. The SOLO program was then employed to calculate the stage 1 and stage 2 linear rate constants (and associated data) for all twenty-two tests in this study, for the temperature range 520°F to 680°F (271°C to 360°C).

3. Summary of Test Data

Table 3 summarizes all of the corrosion data obtained from the twenty-two tests. The second-stage rate constants [K(2)] for the temperatures 520°F and 550°F are included in this table for completeness. However, since corrosion thicknesses at these low temperatures were too thin to have reached stage-two kinetics, the K(2) data for these two lowest temperatures have not been included in stage-two analyses. At these low temperatures the constants calculated by the statistical program for stage-two posttransition corrosion kinetics were not significantly different from their stage-one counterparts, which supports the conclusion that stage-two kinetics had not been attained.

---

[2]As can be seen in Appendix A, this choice of the initiation of posttransition kinetics had very little impact on the statistical evaluation of the posttransition data.

The occurrence of a second posttransition corrosion rate raises the concern that additional corrosion could result in a subsequent higher rate. Although the extrapolation to low temperatures and long times results in predictions outside the database for time, the corrosion rate is not directly determined by exposure time. Rather, the corrosion rate is determined by the physical state of the Zircaloy metal and oxide. As discussed in a later section on corrosion mechanisms, this material state is closely correlated with the amount of corrosion that has occurred. The sole exception is the memory effect that decays quickly and this decay is beneficial rather than detrimental. As will be seen below, the autoclave database presented herein covers corrosion thicknesses up to 4.5 mils, which is greater than the corrosion thickness expected in a repository through one million years.

As in the earlier studies, both stage-one and stage-two linear rate constants appear to follow an Arrhenius-type temperature dependence. Figure 3 shows the natural logarithm of both linear rate constants plotted as a function of the inverse of the absolute temperature. From this figure and the detailed analyses of this plot shown by the data in Appendix A, Table A.2, the following parameters were derived for the stage-one posttransition region: Q/R = -12877 and the pre-exponential constant (B) = 2.46×10^8. The corresponding values for the stage-two kinetic region are -11452 and 3.47×10^7, respectively. Thus, the incremental change in weight obtained by two successive exposure times entirely within the stage-one linear regime [$\Delta\Delta W(1)$] is given by:

$$\Delta\Delta W(1) = K(1) \times \Delta t = 2.46 \times 10^8 \exp[-12877/T] \times \Delta t, \quad [6]$$

and the corresponding weight change for the second-stage linear corrosion is

$$\Delta\Delta W(2) = K(2) \times \Delta t = 3.47 \times 10^7 \exp[-11452/T] \times \Delta t \quad [7]$$

where Δt is the change in time (days) between two successive exposures times entirely within the stage-one or stage-two kinetic regimes and $\Delta\Delta W$ is the weight gain (mg/dm^2) generated between these two exposure times. Since K(2) is always equal to or slightly greater than K(1), and it is assumed that the Zircaloy cladding on the expended fuel elements will be in the posttransition kinetic region upon disposal, Equation [7] will be used to estimate the extent of additional corrosion due to geologic repository exposure. Thus, the use of this equation for all cladding is conservative.

Equations [6] and [7] are known to be valid within the database used for their generation, which is up to approximately 4.5 mils of oxide film. As shown below, extrapolation beyond the limits of the high-temperature database is not needed to estimate the corrosion of Zircaloy-clad naval fuel after disposal in a repository for one million years, which eliminates concerns that there could be changes in the corrosion kinetics for thicker oxides.

4. Application to Repository Conditions

Prior to applying Equation [7] to the Yucca Mountain Repository environment, it is of interest to compare Equations [6] and [7] with the eight earlier models used to estimate the extent of corrosion for the tuff repository conditions. Table 4 is a copy of Table 1 with two additional rows for the results of calculations with Equations [6] and [7].

For the time and temperature shown in Table 4, Equation [6] predicts an additional oxide film growth of ~1.1 mils (which is in line with the other values in this table) whereas Equation [7] produces an oxide film thickness growth of ~3.5 mils. These calculations demonstrate that the use of Equation [7] is more conservative than any of the eight models described above or than the use of Equation [6] for this application.

Figure 4A shows what, at present, is considered to be a conservative temperature profile for naval fuel disposal in the Yucca Mountain Repository facility. Currently, it is anticipated that the inner container could be breached, and the fuel cladding exposed to an aqueous environment, in the period ~1000 to 5000 years after depositing the fuel assembly in the Yucca Mountain Repository. It is assumed that all spent fuel cladding will be in the stage-two linear kinetic regime upon disposal, which is an upper bound on the corrosion rate. As an additional conservative factor, the corrosion calculations shown in Figure 4B initiate at 1000 years after disposal and continue for a total exposure of one million years. An additional oxide film thickness of~0.14 mils is projected for this history.

There have been several additional algorithms reported in the literature for the oxidation of Zicaloy at elevated temperatures. For example, Boase and Vandergraaf [REFERENCE 59] show an Arrenhius-type plot of rate constants compiled from various documents (some unpublished) with wet and dry air and steam in the temperature range ~298°C to 725°C (~570°F to 1340°F). Similarly, Suzuki and Kawasaki [REFERENCE 60] report on the oxidation of Zircaloy in moist air in the temperature range 350°C to 500°C (662°F to 932°F). Einziger [REFERENCE 61] generated an equation for Zircaloy oxidation based upon the work of the previous two references. The results of these studies were not included in the comparisons of Table 4 because of differences in test conditions, i.e., temperature or environment. Inclusion of these reported corrosion rates would not have altered the results of this study, despite the differences in test conditions. Van Swam and Shann [REFERENCE 62] employed the MATPRO corrosion model [REFERENCE 63] to compute out-of-reactor comparison values for their in-reactor measurements. MATPRO calculations conducted for our anticipated repository conditions generate estimates that fall in the middle of the range of values shown in Table 4. For all conditions discussed to date, including the information presented above in references 59-63, Equation [7] of this report produces the most conservative estimate of additional oxide buildup on spent Zircaloy-clad fuel assemblies due to long-term exposure to expected geologic repository conditions. These maximum corrosion rates are due to the underlying database that includes the thickest corrosion films reported to date (up to 4.5 mils).

There is one additional degree of conservatism implicit in the above computations. All calculations have been conducted with the assumption that the environment is water. However, examination of Figure 4A indicates that after breaching (assumed at 1000 years) a considerable period of time is spent above 100°C. Long-term autoclave data have shown that corrosion of Zircaloy in the steam phase is not as aggressive as corrosion in water at the same temperature (see Figure 5). Thus, the use of water autoclave data for the entire exposure time adds another degree of conservatism.

5. Postirradiation Corrosion in Autoclaves

The predictions for the additional corrosion on the Zircaloy cladding during repository disposal presented above were based on isothermal autoclave testing of nonirradiated specimens. The corrosion of cladding that has experienced appreciable irradiation exposure prior to disposal in the repository may be accelerated, especially for the posttransition kinetic regime. At the present time it is uncertain how long this accelerated in-reactor corrosion rate will persist when

transferred to an ex-reactor corrosion environment, but sufficient data are available to bound the effect.

Garzarolli et al. [REFERENCE 16] conducted an experiment to determine how rapidly the enhanced corrosion rate observed in-reactor would decrease to that anticipated from ex-reactor (autoclave) data. The authors found that samples of cladding from a BWR that were irradiated at an estimated temperature of 554°F (290°C) continued to corrode at the irradiated rate for the first ten days in an autoclave at 536°F (280°C). In the time frame from 10 to 110 days the rate continued to decrease until, at 110 days, it became close to that measured in autoclave testing of nonirradiated specimens. When exposed to higher temperatures in autoclaves (572-662°F; 300-350°C) the specimens were found to attain the ex-reactor rate quickly. At the highest autoclave temperature there appeared to be no "memory" effect of the prior irradiation exposure, i.e., the measured corrosion rate agreed very favorably with the ex-reactor rate from the onset of the high-temperature postirradiation autoclave exposure.

Somewhat different results were obtained with specimens from cladding taken from PWRs. In one batch of irradiated specimens tested in autoclaves at temperatures up to 617°F (325°C), the corrosion rate measured after the first cycle of exposure in the autoclave was a factor of 20 greater than the nonirradiated corrosion rate but decreased rapidly to a factor of 2 or less during subsequent autoclave exposures. The test was terminated after 180 days in the autoclave. It is not known whether additional long-term autoclave exposure would have resulted in the convergence of the postirradiated and nonirradiated corrosion rates, as observed with the BWR specimens for shorter exposure times. At a higher autoclave temperature (662°F; 350°C) the corrosion rate for the PWR specimens agreed very well with the expected nonirradiated corrosion rate. In all cases, the effect of irradiation was reduced to a factor of two or less on or before 110 days of postirradiation exposure at 280°C. The technical basis for this memory effect and the factor of two for postirradiation corrosion are discussed in more detail in a later section.

Cheng et al. [REFERENCE 58] also investigated postirradiation corrosion performance of Zircaloys. However, they removed the in-reactor oxide film and pickled the surface on almost all of their samples before postirradiation autoclave exposure. The oxide was removed because they were concentrating on determining the effect of irradiation on corrosion rates through irradiation-induced dissolution of second-phase particles in the metal. With the exception of two of the weld metal samples, all samples postirradiation tested at 316°C (600°F) corroded at essentially the same rate as nonirradiated samples, despite the irradiation-induced changes in microstructure and dissolution of alloying elements into the zirconium matrix, which Cheng et al. confirmed. Two of the weld metal samples postirradiation tested at 316°C corroded at higher rates than the other samples. This was attributed to the strong susceptibility of the small weld-metal precipitates to an irradiation-induced dissolution. There was no explanation as to why some weld metal samples corroded at an accelerated rate and some at the corrosion rate of nonirradiated material. However, all base metal samples corroded at the nonirradiated rate, not showing the memory effect reported by Garzarolli. This would suggest that the memory effect at 316°C (600°F) is associated with the effect of irradiation on the oxide films rather than on the base metal. This interpretation is somewhat different from that given by Cheng et al. The modified interpretation is necessary to reconcile the posttransition corrosion observations of both Garzarolli and of Cheng for postirradiation testing with and without the in-reactor oxide removed.

Cheng also postirradiation- tested samples at 400°C (752°F) and observed accelerated corrosion. For samples with the oxide removed, the corrosion rate was initially high but decreased with postirradiation exposure. This decrease in rate was associated with precipitation of alloying elements during postirradiation testing, which occurred at 400°C but not at 316°C. One sample postirradiation tested at 400°C with the in-reactor corrosion film left on behaved

differently from the samples postirradiation tested at 400°C with the in-reactor corrosion films removed. The sample with the in-reactor corrosion film left on initially corroded at a slow rate that was more like the in-reactor rate than the 400°C rate, suggesting that the character of the oxide initially controlled the rate in this case. After some time, the corrosion rate for the sample with the in-reactor oxide left on increased to a similar rate as the postirradiation rate of the samples with the in-reactor oxides removed.

The testing of Garzarolli et al. and Cheng et al. suggest that there are two postirradiation time-dependent effects of in-reactor irradiation on postirradiation corrosion rates. The first effect is on the oxide. This effect is a postirradiation corrosion-rate acceleration that decays relatively rapidly, at least rapidly compared to repository times, to less than a factor of two of the nonirradiated posttransition corrosion rate at 316° and lower. The second effect is on the metal. At relatively high temperatures the alloying elements that became supersaturated by the irradiation-induced dissolution begin to precipitate in a unique microstructure that increases the corrosion rate at 400°C. This unique microstructure and the associated acceleration in corrosion rate do not occur at 316°C. The temperature dependence on postirradiation microstructural changes at high temperatures has been observed by other investigators. For repository conditions (Figure 4A) the temperatures are never high enough to induce such microstructural changes. Therefore, the testing at 316°C and below by both Garzarolli et al. and by Cheng et al., despite Cheng's removal of the oxide, support the assumption that the postirradiation repository corrosion rates will be within a factor of two of the nonirradiated posttransition corrosion rates reported and modeled above.

These postirradiation corrosion test results suggest that it is possible for PWR Zircaloy cladding in a repository to experience an enhanced corrosion rate over that predicted from autoclave test data. A conservative treatment is to assume that the corrosion rate at the low repository temperatures will not converge to the preirradiation rate, even after one million years in the repository. This can be reflected by applying a factor of two to the corrosion rate. Using this conservative factor of two increase for the entire exposure time, the final additional increase in the oxide film thickness of Zircaloy cladding interred in the Yucca Mountain Repository is anticipated to be twice that estimated by Equation [7], for a total of 0.28 (or~0.3) mils. This small increment in oxide film thickness is insignificant compared to the Zircaloy cladding thickness.

EFFECT OF CHEMISTRY

The autoclave corrosion data discussed above have been generated in water chemistries where every attempt has been made to eliminate, or at least control to a very low level, all sources of contaminants in the test environment. In contrast, the ground water in the Yucca Mountain repository will include an unspecified and variable chemistry. To generate a plausible composition for the ground water anticipated at the repository, a deep well was drilled in the vicinity of Yucca Mountain (henceforth designated as the J-13 well) and the water analyzed for ionic species. The analysis results for the J-13 well water are shown in Table 5. The chemical composition of the J-13 well water is taken as representative of the ground water environment in the Yucca Mountain Repository.

It appears that, in general, the concentrations of the ionic species in J-13 well water are too low to have an adverse effect on the Zircaloy corrosion behavior. The following is a brief discussion of the known effects of the more-aggressive ionic species in the J-13 well water:

1. Fluoride (F^-)

The fluoride ion is probably the most aggressive of the ionic species; in sufficient quantity it will prevent the formation of the protective oxide and lead to a rapid attack of Zircaloy. Berry [REFERENCE 31] has shown that at concentrations in excess of 100 ppm the fluoride ion will degrade the normally excellent corrosion resistance of Zircaloy but concentrations below this value will not influence corrosion performance. If maintained at this level, the 2 ppm of F^- found in J-13 well water should have no effect on the Zircaloy corrosion behavior.

2. Chloride (Cl^-)

The combination of Zircaloy and chloride ions results in the possibility of local attack by pitting and stress corrosion cracking. The effect of the chloride can be magnified by the presence of ferric (Fe^{+3}) or cupric (Cu^{+2}) ions [REFERENCES 32,33]. However, there is no known readily-available source of copper whereby cupric ions could contaminate the ground water in the repository. The exception would be if the repository containers had a high copper concentration. There is a small amount of copper in the crud on fuel elements, but this has not accelerated corrosion of fuel cladding during service.

There could be sources of iron in the repository from the disposal containers and repository construction. It has been shown that room temperature additions of 100 ppm ferric ions to a solution of concentrated acidic chloride will increase the corrosion rate of a commercial zirconium-base alloy by a factor of 25 and cause a pitting attack [Reference 34]. However, Maguire [REFERENCE 64] has shown that pitting of zirconium in acidic ferric chloride solutions will not occur above a pH of 3 and that this behavior is consistent with the Pourbaix stability diagram for iron that shows that the ferric ion (Fe^{+3}) is not stable above a pH of 3. Thus, if the pH of ground water remains above 3 there is little chance of generating a ferric-chloride-induced pitting attack of the cladding. J-13 well water has a pH of 7.4.

3. Lithium (Li^+)

In neutral or acid solutions lithium has no detrimental effect on the corrosion resistance of Zircaloy. In basic solution lithium can form lithium hydroxide (LiOH) which, if in sufficiently concentrated solutions, can have an adverse effect on Zircaloy corrosion performance. However several investigations have shown that a lithium hydroxide concentration of greater than 1000 ppm is required to cause accelerated corrosion [REFERENCES 35-37]. The concentration of lithium ion in J-13 water is only 0.05 ppm, which is well below those levels that could cause concern.

4. pH (H^+)

Cox [REFERENCE 38] reports that the corrosion of the Zircaloys at elevated temperatures is insensitive to the hydrogen ion concentration (pH) in the pH range of 2 to 12. The J-13 water has a measured pH of 7.4, well within these bounds. As indicated above, lithium hydroxide in sufficiently high concentrations (>pH 12) can greatly accelerate the Zircaloy corrosion kinetics and other strong alkalis (e.g., sodium, potassium and calcium) can have similar, but smaller, effects at these highly basic pH values [REFERENCES 37,39]. These conditions are not credible because pH levels in the J-13 water would have to concentrate by a factor of 10^5 (100,000 times), which is not a very likely event.

The Pourbaix diagram calculations of REFERENCE 40 suggest that the base metal, zirconium, has an excellent corrosion resistance to pure water at temperatures in the region of 25°C (77°F) over a wide range of pH and electrode potential values. Figure 2 on page 227 of REFERENCE 40 shows the various stability and corrosion domains generated for zirconium at 25°C (77°F). The region marked as "immunity" in this diagram indicates the area wherein the metal does not react with water; it is completely noble in this domain. In the region titled "passivation" the metal becomes coated with an oxide (ZrO_2) that virtually prevents all direct contact between the metal and the solution. The exposed cladding surfaces will be in this region. This diagram shows the extensive range of pH and electrochemical potential where the zirconium passivated surface should not experience a corrosion attack. Due to the fact that the Zircaloys are dilute alloys of zirconium, and that the passivation product (ZrO_2) is virtually the same on all dilute zirconium alloys, this diagram can be employed to represent Zircaloy behavior, as well.

5. Other Ions

By virtue of their low concentrations, the other ions listed in Table 5 for J-13 water also are not anticipated to degrade the Zircaloy corrosion performance. In fact, at concentrations well above those in the J-13 water both the nitrate (NO_3^-) and sulfate ($SO_4^=$) ions may be beneficial in that they can inhibit pitting in the presence of chloride ion.

The discussions in this section suggest that the ionic constituents in the J-13 well water, in the measured concentrations and pH levels, would have no detrimental effect on the Zircaloy corrosion behavior in the Yucca Mountain repository, relative to that observed in autoclave testing. In addition, most of the testing discussed in this section was conducted with bare (i.e., unfilmed) zirconium or zirconium-alloy specimens whereas the spent fuel elements should have a protective passive corrosion film upon disposal. This different surface can have a pronounced affect on the chemical interactions discussed herein.

MICROBIOLOGICALLY INFLUENCED CORROSION

The term microbiologically influenced corrosion (MIC) is commonly used to designate that type of corrosion attack associated with microbial activity at metal surfaces. As indicated by Little and Wagner [REFERENCE 41], MIC is a form of localized corrosion that can result in pitting, selective leaching of alloys, crevice corrosion, underdeposit corrosion, and enhanced erosion corrosion. Little and Wagner divided the reactions between biofilms and metal surfaces into the following general categories: sulfide, acid, hydrogen and ammonia production, and metal deposition. The two major forms of MIC for materials being considered for containment vessels in mined geological repositories are sulfide attack through the action of sulfate-reducing bacteria (SRB) and organic acid production by secretion of certain bacteria.

McNeil and Odom [REFERENCE 42] have indicated, by thermodynamic calculations, that zirconium would not be affected by SRB. Considering the tolerance that Zircaloy has for a wide range of pH values, it is unlikely that production of weak organic acids will have an adverse effect on the passivation of Zircaloy by the ZrO_2 film.

PERSPECTIVE ON EXTRAPOLATING CORROSION RATES TO REPOSITORY CONDITIONS

Introduction

The analysis of the data presented above uses a standard thermal dependency to extrapolate to the low temperatures and long times associated with repository corrosion. The uncertainty in this thermal dependency, that is, the uncertainty in the thermal activation energy, and its impact are calculated by standard statistical methods. Implicit in this extrapolation is the assumption that the rate-controlling process remains unchanged between the test-temperature range and the application-temperature range. To better understand the impact of the extrapolation, physical aspects of the corrosion process are reviewed.

The corrosion rate of Zircaloy in water is limited by the slowest of the basic corrosion steps: dissociation of water into oxygen and hydrogen ions, diffusion of oxygen ions through the oxide film, oxidation of the Zr metal, diffusion of electrons through the oxide, and hydrogen-ion reduction by the electrons at the water-to-oxide interface. At temperatures for current testing, that is, above about 450°F, diffusion of oxygen ions through the oxide film is rate limiting [REFERENCE 43]. In extrapolating to lower temperatures, one of the other basic steps could become rate limiting, which would decrease the corrosion rate to less than predicted by the extrapolation. In that case, projections based on oxygen-ion diffusion through the oxide would be conservative. Therefore, analyses herein are based on the assumption that oxygen-ion diffusion is rate limiting in the repository. That is, if one of the other steps in the currently considered process had a high enough temperature dependency that it displaced oxygen-ion diffusion as the rate limiting step, the extrapolation to repository temperatures used herein would be conservative. The only risk that more corrosion will occur than predicted by the extrapolations based on a thermal activation energy is that a new more-rapid corrosion mechanism becomes active.

The corrosion process usually is described and modeled as a function of time. However, changes in the corrosion rate or the mechanism occur due to physical changes that are occurring r the environment. Therefore, it is important to understand what changes might influence the corrosion mechanism. Two aspects of the extrapolation to low temperatures are discussed. Both are based on considering what physical changes are occurring with corrosion and how these changes might affect the extrapolation. First, in a repository environment, the active mechanism controlling the corrosion rate is expected to be as closely correlated with the amount of additional corrosion that occurs in the repository as with the time in the repository. Therefore, understanding corrosion for the amount of additional corrosion expected in the repository is just as important as obtaining data for the amount of time expected in the repository, which can not be achieved. This important feature of corrosion supports extrapolation of available models for corrosion to repository conditions as long as the database on which the models were built extends to the corrosion thicknesses expected in a repository. Second, the temperature dependencies of the physical changes that may occur are considered to determine if there is any evidence that a new more-rapid corrosion mechanism could occur at repository conditions. This review is needed to minimize the risk that extrapolation to repository conditions will not conservatively represent the expected repository corrosion mechanism.

This reliance on thickness of corrosion rather than time is established by considering three broad primary categories of parameters to which the corrosion rate is sensitive. As appropriate, thermal dependencies also are considered. Early studies showed that corrosion is sensitive to the alloy design. The most important such feature is the alloy chemistry, and the associated type and size distribution of second-phase particles, which are controlled primarily through heat-

treatment schedules during manufacturing. Subsequent work showed that corrosion of Zircaloys also is sensitive to the environment, both to water chemistry and to neutron irradiation. Finally, research has shown that corrosion rate is sensitive to oxide thickness. Each of these three categories, Alloy Design, Service Environment, and Oxide Thickness, reflects the effects of other more fundamental parameters. The primary ones are reviewed below.

Alloy Design

Zirconium alloys in world-wide nuclear-core applications, principally the Zircaloys, are alloyed with tin, iron, chromium, and nickel, and in some cases niobium. Except for tin, these elements are not very soluble and form second-phase particles. The type and size distribution of these particles are determined by alloy chemistry and processing, mainly heat treatments. Once established during manufacture, alloy-design features are only changed by exposure to high temperatures or to irradiation flux. During exposure in reactor cores, the temperatures are not high enough to induce significant microstructural changes. However, the irradiation field can induce significant changes. In particular, at low irradiation temperatures, second-phase particles are transformed from crystalline form to amorphous form. At intermediate temperatures, iron, chromium, and nickel are ejected and diffuse out of the otherwise thermally stable second-phase particles [REFERENCES 44-46]. Reprecipitation may occur for irradiation at higher reactor temperatures [REFERENCE 46]. These reactor-service changes in microstructure increase the corrosion rate of Zircaloys, and may be the basis for the short-term postirradiation factor of two in corrosion rate in the model described elsewhere in this paper.

Alloy design and changes during reactor exposure are fixed on entering repository service. The primary potential impact on subsequent corrosion is the reprecipitation of the alloying elements iron, chromium, and nickel, which the irradiation causes to be supersaturated in the zirconium matrix. In development of zirconium alloys, it was found that corrosion rates decreased with annealing and precipitation of these alloying elements, with the optimum amount depending on the in-reactor service conditions. The important observation is that precipitation generally reduces corrosion to some optimum amount of precipitation. As discussed below, repository temperatures will be too low to reach this optimum. Therefore, repository exposure is expected to alter the alloy microstructure in a direction to improve corrosion resistance, although perhaps by an insignificant amount.

Repository Service Environment

The expected repository environment will not include sufficiently high temperatures nor neutron irradiation flux to significantly alter alloy-design features, primarily the microstructural character of the second-phase particles and the associated amounts of iron, chrome, and nickel in solution. The most commonly used parameter to estimate the effect of thermally induced changes in microstructure on corrosion is the $\sum A_i$ parameter, as defined by Garzarolli [REFERENCE 47]. The $\sum A_i$ parameter is a measure of the effect of time at temperature on Zircaloy microstructure and of the associated effect on corrosion. The thermal activation energy in Garzarolli's analysis is Q/R = 40,000K. Based on this value of Q/R and the repository thermal history of Figure 4A, the integrated $\sum A_i$ parameter for the full repository life is expected to be approximately 1×10^{-30} h. As shown in Figure 6, essentially all the annealing occurs during the first 50 years, long before any water might access zirconium-alloy surfaces in a container. This $\sum A_i$ parameter must be significantly greater than 10^{-20} h to affect corrosion. Therefore, the amount of annealing that will occur during repository service is orders of magnitude less than required to significantly affect thermal corrosion. To the small extent that this effect occurs for irradiated material, it will restore

the material condition toward that of nonirradiated material, which will decrease the corrosion rate, as discussed below.

The factor of two in corrosion rate reported by Garzarolli et al. [REFERENCE 16] and used in the above model for repository corrosion reflects the impact of irradiation-induced changes in the material condition on postirradiation corrosion rates. There is no irradiation enhancement during pretransition corrosion but irradiation during pretransition corrosion enhances corrosion rates after the pretransition period. That is, the material has a memory of previous exposure through the changes in the material condition. After a change in exposure conditions, in flux and temperature, the material condition and the corrosion rate slowly change to reflect the new exposure conditions. This is important for repository service because it leads to the conclusion that the postirradiation corrosion rates will slowly decrease toward those measured in autoclaves. More important, no increase in corrosion rate during repository service is expected. Experimental evidence of the memory effect and its decay with time are illustrated in the results of corrosion tests performed in the Advanced Test Reactor (ATR) on Zircaloy-4 corrosion coupons.

Figure 7a shows the corrosion of a Zircaloy-4 coupon exposed in ATR at about 520°F for 2500 days, initially at high flux with several decreases in flux to one third of the initial flux at the end of the irradiation, as shown in the irradiation history provided in Figure 7b. Figure 7a also shows the corrosion of coupons exposed to the irradiation history of Figure 7c, a nearly constant high-flux level that is comparable to the average level of Figure 7b. As the data for the coupon corresponding the history of Figure 7b show, the irradiation flux level has no effect on the corrosion rate during the pretransition period of approximately the first 1000 days. However, after this pretransiton period, the corrosion rate increases beyond what would be expected for the irradiation flux level during this time, based on isoflux tests. In fact, the rate is higher at this time than the nearly constant high-flux data of samples irradiated with the history of Figure 7c. Finally, after another 500 days, the corrosion rate has decreased to a rate that is now less than the rate of the samples of Figure 7c , even though those samples have experienced about the same average irradiation flux level. The important memory-related results of this test are that: 1) the initial high-flux period during the first 500 days was not reflected in the corrosion rate until about 1200 days, when the sample left the pretransition period, and 2) the decrease in flux to below that of the flux of the other samples, just as the sample left the pretransition period at about 1200 days, was not reflected in the corrosion rate until about 500 days later at 1700 days, after which the corrosion rate became less than that of the other samples. This demonstrates that decreases in neutron irradiation flux are not initially reflected in corrosion rate; but after additional corrosion of 1μm to 2μm, corrosion rates decrease.

This memory effect also is illustrated in a coupon initially irradiated for about 100 days at a high temperature (680°F) and then irradiated at a low temperature (520°F). The control samples are the same ones as for the above illustration, being irradiated at low temperature throughout their exposure. The result is shown in Figure 8a. During the ~100 days at 680°F approximately ten microns (0.4 mils) of corrosion occurred. Immediately upon lowering temperature to 520°F and increasing flux, as shown in Figure 8b, the corrosion rate deceases to a lower rate than expected for the existing corrosion thickness, as shown in Figure 8a, which also shows the corrosion rate for coupons exposed isothermally at 520°F. Approximately 1000 days at 520°F are required before the corrosion rate of the temperature-shifted sample becomes similar to that of isothermally exposed samples. During exposure at 680°F much of the irradiation effect on the Zircaloy-4 is annealed relatively quickly. As a result, the corrosion rate immediately following the temperature change to 520°F initially is more representative of nonirradiated material than material aerated at 520°F. After about 1000 days at 520°F, irradiation damage produces a material representative of material irradiated isothermally at 520°F and the corrosion rate also

becomes the same. A similar memory effect, out-of-pile, has been reported by Beie et al. [REFERENCE 56].

A possible explanation for this memory effect is as follows: The corrosion rate is determined by the diffusion of oxygen ions through the thin barrier oxide at the metal-to-oxide interface. Initially after a change in flux or temperature, oxygen ions diffuse through oxide formed at the previous conditions. If the existing oxide is more damaged than oxides irradiated at the existing conditions, as is the case for the flux-shifted sample of Figure 7, a relatively fast diffusion rate occurs. If the existing oxide is less damaged than oxides irradiated at the existing conditions, as is the case for the temperature-shifted sample of Figure 8, a relatively slow diffusion rate occurs. As new oxide forms, its character and resistance to diffusion of oxygen ions is determined by the new conditions. After a change in conditions, the corrosion rate slowly changes to reflect the new conditions. A similar behavior is expected in a repository. Initially, the corrosion rate will be higher than expected for nonirradiated material, as observed by Garzarolli. Eventually the corrosion rate will revert to the corrosion rate for nonirradiated material.

The rapid decay in corrosion rate from the in-reactor rate to that for nonirradiated material is not due to normal thermal annealing, as estimated by the $\sum A_i$ parameter. Garzarolli's postirradiation corrosion tests showed that less than 110 days at 280°C is required to reduce the corrosion rate to within a factor of two (or less) of the nonirradiated corrosion rate. One hundred and ten days at 280°C corresponds to an $\sum A_i$ parameter of only 10^{-30} h. Therefore, the rapid decrease in postirradiation corrosion rate probably is due to a different effect than that associated with thermal annealing. Although this effect has not been identified, the effect on repository corrosion is known. Since repository fuel will be at temperatures similar to Garzarolli's 280°C postirradiation testing for on the order of 100 years (see Figure 4A), the postirradiation corrosion rate enhancement will be well below the factor of two assumed in the analyses herein. Garzarolli also reported the additional corrosion thickness for postirradiation corrosion rate to decrease to within a factor of two of the nonirradiated rate. By two micrometers (μm) of additional oxide, all samples had a rate within a factor of two of the nonirradiated rate. Two micrometers (~0.08 mils) is not significant for repository corrosion performance.

In summary, changes to zirconium-alloy microstructures during repository service, other potential memory effects, and the presence of dissolved chemical species in the water (discussed earlier) are not expected to be significant enough to result in a different dominant corrosion mechanism, nor to alter the corrosion rate for the established corrosion mechanisms. Any material changes that might occur are expected to decrease the corrosion rate due to the slow annealing of irradiation damage.

Oxide Thickness

Uniform oxide thickness correlates to corrosion directly and indirectly. The direct effect is the barrier that the oxide provides against the diffusion of oxygen ions through the oxide to the metal. However, this barrier breaks down after about two microns of oxide thickness, after which only the indirect effect of oxide thickness is important. The indirect effect is through the correlation between the oxide thickness and changes in other parameters that influence corrosion. In posttransition corrosion, the primary indirect factors are the stresses in the oxide and metal and the concentrations of oxygen and hydrogen in the metal close to the oxide, each of which correlates to the oxide thickness. In particular, compressive oxide stresses reduce the corrosion rate [REFERENCE 48], perhaps by stabilizing the tetragonal oxide phase at the oxide-to-metal interface [REFERENCE 49]. High concentrations of oxygen and hydrogen in the metal substrate, especially when sufficient hydrogen is present to precipitate hydride phase, increase the corrosion rate [REFERENCE 50]. The mechanism by which stress or the increased hydrogen

and oxygen concentrations affect the corrosion rate is not known. The important feature is that the stress and the amount of hydrogen and oxygen increase are correlated to oxide thickness increase, not to time. The exception is for creep processes, which in principle could affect corrosion. The potential for creep to affect corrosion is discussed below.

The increase in hydrogen concentration in the metal due to corrosion has been shown to be proportional to the amount of oxidation. For in-reactor corrosion, the ratio of increased hydrogen concentration to the amount of oxidation decreases with decreasing temperature [REFERENCE 51]. Out-of-pile, the ratio of hydrogen concentration increase to amount of oxidation is insensitive to temperature. Therefore, as long as the expected repository corrosion thicknesses are within the oxide thicknesses in the current database, the effects of hydrogen concentrations on the corrosion mechanism are expected to be predicted by the current models.

The oxygen and hydrogen concentrations in the metal close to the oxide also are influenced by diffusion into the metal. If diffusion is relatively fast, the concentrations close to the oxide will change little with increasing corrosion, in which case the concentrations will not be a function of either oxide thickness or time. At autoclave test temperatures, hydrogen diffuses more rapidly than corrosion occurs. Unless there is a temperature or stress gradient to bias diffusion, hydrogen will not build up at the oxide interface. The opposite is true for oxygen. Whether there is a change in going from autoclave test conditions to the repository depends on the relative activation energies for diffusion of oxygen and hydrogen in the zirconium lattice, and possibly on the hydrogen supercharging capability of the lattice. Since the activation energy for hydrogen diffusion is less than the activation energy for corrosion and the hydrogen diffusion is rapid at autoclave temperatures [REFERENCE 52], the extrapolation to the lower repository temperatures will not result in an increase in the concentration of hydrogen in the metal close to the oxide. The activation energy for oxygen diffusion in the metal (approximately 45 kcal/mol, REFERENCE 54) is greater than the activation energy for corrosion, but the oxygen diffusion rate at the autoclave test temperatures of the existing database is slow enough that oxygen concentrates at the oxide-to-metal interface. Extrapolation to lower temperatures will result in continued concentration of oxygen in the metal at the oxide-to-metal interface, increasing the gradient of oxygen concentration into the metal. If this were to result in a new rate-limiting step at low temperatures, that is, if corrosion were to become limited by the diffusion of oxygen into the metal, the corrosion rate would be less than predicted by the extrapolation used herein based on the corrosion activation energy at existing autoclave test temperatures. Therefore, use of the herein-proposed activation energy for extrapolation to repository temperatures is conservative.

Stress in the thin protective oxide layer can affect the corrosion rate. Compressive stresses decrease the corrosion rate, perhaps by stabilizing the tetragonal oxide phase [REFERENCE 49]. Oxidation in the repository will increase the oxide compressive stresses, as oxidation does in autoclave tests. These stresses can be relieved by creep in the metal substrate, both in the repository environment and in autoclave tests. In the absence of a significant irradiation field in a repository, the relative creep rates in the repository and in autoclave tests depends on the thermal activation energy for creep, which is on the order of 70 kcal/mol [REFERENCE 53]. Since this is greater than the activation energy for corrosion, extrapolation to low temperatures will decrease the relative amount of stress relaxation in the oxide compared to the amount of creep that is reflected in the autoclave test database. This will tend to maintain the oxide compressive stresses, which reduce the corrosion rate. The activation energy for oxide creep is not well known. For CaO-stabilized oxide the activation energy is about 94 kcal/mol [REFERENCE 55]. Extrapolation to lower temperatures will result in a decrease in creep rate faster than the decrease in corrosion rate, which also will tend to maintain the compressive stresses in the oxide, which reduce the corrosion rate.

In summary, the extent of the current database for autoclave corrosion, in terms of oxide thickness, provides confidence that key parameters associated with corrosion are adequately covered. Based on a review of the thermal responses of potential contributors to the corrosion processes, extrapolation to repository conditions is not expected to result in nonconservative predictions of corrosion. Therefore, there is an acceptably low risk that the extrapolation to lower temperatures and longer times will be significantly affected by the repository service environment.

UNCERTAINTIES IN ESTIMATES OF ZIRCALOY CORROSION

The above estimates of the corrosion of Zircaloy for long periods of time at low temperatures (FIGURE 4B) do not include conservatism to account for uncertainties. There are several ways to address this issue and more is involved than just the uncertainty in the corrosion rate. Uncertainty in the input to the corrosion calculation, for example, uncertainty in the thermal history or environmental conditions, also is important. Therefore, the appropriate conservatism can not be addressed for this limited discussion of Zircaloy corrosion. In the end, it is the conservatism in the final outcome, for example, release to the environment or risk of criticality, that is important. Nevertheless, some perspective can be provided.

The uncertainty in the extrapolation from the database temperatures of about 600°F and above to repository temperatures is estimated through calculation of the uncertainty in the thermal activation process, Q/R, as provided above. The upper 95-percent confidence limit of the corrosion rate was used in combination with the estimated repository thermal history, which has its own conservatism, to estimate the amount of Zircaloy corrosion that would occur after one million years in the repository (see Appendix A for details). This value was found to be 0.63 mils, compared to 0.14 mils calculated above using the best-estimate corrosion rate and the same thermal history. This estimate is not a recommended method of handling conservatism but is provided for perspective. The appropriate method for handling conservatisms should be addressed in the context of the overall repository analysis procedure.

DISCUSSION AND CONCLUSIONS

It has been shown that, employing a conservative estimate of the Zircaloy corrosion kinetics, the additional oxide film growth on Zircaloy cladding of spent naval fuel assemblies in the Yucca Mountain Repository for a million years will be small (~0.3 mils), even when an additional conservative factor of two enhancement of the rate is used to account for the prior irradiation exposure of the cladding. This small increment in oxide film thickness should pose no problem to the integrity of the Zircaloy cladding. Chemical contaminants in the ground water and microbiologically influenced corrosion, at currently anticipated levels, should have no adverse effect on repository disposal of Zircaloy. The current understanding of Zircaloy corrosion supports extrapolation from the database provided to the relatively low temperatures and very long times for repository service. Direct measurement of the Zircaloy corrosion behavior at the anticipated repository temperatures is not amenable to experimentation due to the long times involved. However, Zircaloy specimens are being included in the Lawrence Livermore National Laboratory test program to evaluate the corrosion of various materials in J-13-type water [REFERENCE 57].

ACKNOWLEDGMENTS

The authors wish to acknowledge the direction supplied by, and the many helpful discussions held with, Mr. Bruce F. Kammenzind. The aid of Dr. W.J. Duffin in compiling the chemistry data is also appreciated. The assistance of Ms. Cheryl Hall in all phases of data collection, collation and transmittal is also acknowledged and the use of Figures 4B and 7-9, supplied by Dr. Erik Mader, is likewise appreciated.

REFERENCES

1. Bryner, J. S., "The Cyclic Nature of Corrosion of Zircaloy-4 in 633 K Water," Journal of Nuclear Materials, Vol. 82, 1979, pp. 84-101

2. Thomas, D. E. in *Metallurgy of Zirconium*, B. Lustman and F. Kerze, Eds., McGraw Hill, New York, 1955, Chapter 11, pp. 608-640

3. Kass, S., *Proceedings*, U.S: Atomic Energy Commission Symposium on Zirconium Alloy Development, Castlewood, Pleasanton, CA, 12-14 Nov., 1962, pp. 1-1 to 1-44, WAPD-T-1549

4. Kass, S. in *Corrosion of Zirconium Alloys*, ASTM STP 368, American Society for Testing and Materials, 1964, pp. 3-27

5. Thomas, D. E., *Proceedings*, International Conference on the Peaceful Uses of Atom Energy, Vol. 9, United Nations, Geneva, 1955, pp. 407-413

6. Chirigos, J. N. et al, *Proceedings*, Fuel Element Fabrication with Special Emphasis on Cladding Materials," Vol. 1, Academic Press, New York, 1961, pp. 19-55

7. Kass, S., *Corrosion*, Vol. 23, No. 12, Dec. 1967, pp. 374-378

8. Draley, J. E. et al, *Proceedings*, Third International Conference on the Peaceful Uses of Atomic Energy, United Nations, Geneva, 1964, Vol. 9, pp. 470-478

9. Kass, S., and Kirk, W. W., *Transactions*, American Society for Metals, Vol. 55, No. 1, March 1962, pp. 77-100

10. Kass, S., "The Corrosion and Hydrogen Pickup of Electron Beam Welded Nickel-Free Zircaloy-2 and Zircaloy-4," WAPD-TM-533, Westinghouse Electric Corporation, March 1966

11. Hillner, E., "Corrosion of Zirconium-Base Alloys - An Overview," *Zirconium in the Nuclear Industry*, ASTM STP 633, A. L. Lowe, Jr. and G. W. Parry, Eds., American Society for Testing and Materials, 1977, pp. 211-235

12. van der Linde, A., "Calculation of the Safe Life Time Expectancy of Zirconium Alloy Canning in the Fuel Elements of the NERO Reactor," RCN Report 41, Reactor Centrum Nederland, Petten, July 1965

13. Dyce, I. H., *Nuclear Engineering*, Vol. 9, No. 98, July 1964, pp. 253-255

14. Dalgaard, S. B., "Long Term Corrosion and Hydriding of Zircaloy-4 Fuel Clad in Commercial Pressurized Water Reactors with Forced Convective Heat Transfer" in Extended Abstracts of the Electrochemical Society, Washington, DC, 2-7 May 1976, Vol. 76-1 Abstract #31, pp. 82

15. Billot, P., Beslu, P., Giordano, A., and Thomazet, J., "Development of a Mechanistic Model to Assess the External Corrosion of the Zircaloy Claddings in PWRs," *Zirconium in the Nuclear Industry: Eighth International Symposium, ASTM STP 1023*, L. F. P. Van Swam and C. M. Eucken, Eds., American Society for Testing and Materials, Philadelphia, 1989, pp. 165-184

16. Garzarolli, F., Jung, W., Schoenfeld, H., Garde, A. M., Parry, G. W., Smerd, P. G., "Waterside Corrosion of Zircaloy Fuel Rods," EPRI NP-2789, December 1982

17. Stehle, H., Kaden, W., and Manzel, R., "External Corrosion of Cladding in PWRs," Nuclear Engineering and Design, Vol.33, 1975, pp. 155-169

18. Peters, H. R., "Improved Characterization of Aqueous Corrosion Kinetics of Zircaloy-4," *Zirconium in the Nuclear Industry: Sixth International Symposium, ASTM STP 824*, D. G. Franklin and R. B. Adamson, Eds., American Society for Testing and Materials, 1984, pp. 507-518

19. Kass, S., "Aqueous Corrosion of the Zircaloys at Low Temperatures," Journal of Nuclear Materials, Vol.29, 1969, pp. 315-321

20. Rothman, A. J., "Potential Corrosion and Degradation Mechanisms of Zircaloy Cladding on Spent Nuclear Fuel in a Tuff Repository," Lawrence Livermore National Laboratory Report UCID-20172, September 1984

21. Johnson, A. B., Jr., "Behavior of Spent Nuclear Fuel in Water Pool Storage," Pacific Northwest Laboratories, Richland, WA, Report BNWL-2256, September 1977

22. Lanning, D. D., Johnson, A. B., Jr., Trimble, D. J., and Boyd, S. M., "Corrosion and Hydriding of N Reactor Pressure Tubes," *Zirconium in the Nuclear Industry: Eighth International Symposium, ASTM STP 1023*, L. F. P. Van Swam and C. M. Eucken, Eds., American Society for Testing and Materials, Philadelphia, 1989, pp. 3-19

23. Graham, R. A., Tosdale, J. P., and Finden, P. T., "Influence of Chemical Composition and Manufacturing Variables on Autoclave Corrosion of the Zircaloys," *Zirconium in the Nuclear Industry: Eighth International Symposium, ASTM STP 1023*, L. F. P. Van Swam and C. M. Eucken, Eds., American Society for Testing and Materials, Philadelphia, 1989, pp. 334-345

24. Garzarolli, F., Jorde, D., Manzel, R., Politano, J. R., and Smerd, P. G., "Waterside Corrosion of Zircaloy-Clad Fuel Rods in a PWR Environment," *Zirconium in the Nuclear Industry: Fifth Conference, ASTM STP 754*, D. G. Franklin, Ed., American Society for Testing and Materials, 1989, pp. 430-449

25. Johnson, A. B., Jr., "Bases for Extrapolating Materials Durability in Fuel Storage Pools," Pacific Northwest Laboratory, Report PNL-SA-24126, December 1994

26. Graham, R. A. and Eucken, C. M., "Controlled Composition Zircaloy-2 Uniform Corrosion Resistance," *Zirconium in the Nuclear Industry: Ninth International Symposium, ASTM STP*

1132, C. M. Eucken and A. M. Garde, Eds., American Society for Testing and Materials, Philadelphia, 1991, pp. 279-303

27. Isobe, T. and Matsuo, Y., "Development of Highly Corrosion Resistant Zirconium-Base Alloys," *Zirconium in the Nuclear Industry: Ninth International Symposium, ASTM STP 1132*, C. M. Eucken and A. M. Garde, Eds., American Society for Testing and Materials, Philadelphia, 1991, pp. 346-367

28. Urbanic, V. F., Choubey, R., and Chow, C. K., "Investigation of Variables That Influence Corrosion of Zirconium Alloys During Irradiation," *Zirconium in the Nuclear Industry: Ninth International Symposium, ASTM STP 1132*, C. M. Eucken and A. M. Garde, Eds., American Society for Testing and Materials, Philadelphia, 1991, pp. 665-682

29. Pecheur, D., Lefebvre, F., Motta, A. T., Lemaignan, C., and Charquet, D., "Oxidation of Intermetallic Precipitates in Zircaloy-4: Impact of Irradiation," *Zirconium in the Nuclear Industry: Tenth International Symposium, ASTM STP 1245*, A. M. Garde and E. R. Bradley, Eds., American Society for Testing and Materials, Philadelphia, 1994, pp. 687-708

30. Garde, A. M., Pati, S. R., Krammen, M. A., Smith, G. P., and Endter, R. K., "Corrosion Behavior of Zircaloy-4 Cladding with Varying Tin Content in High-Temperature Pressurized Water Reactors," *Zirconium in the Nuclear Industry: Tenth International Symposium, ASTM STP 1245*, A. M. Garde and E. R. Bradley, Eds., American Society for Testing and Materials, Philadelphia, 1994, pp. 760-778

31. Berry, W. E., "Effect of Fluoride Ions on the Aqueous Corrosion of Zirconium Alloys," Corrosion of Zirconium Alloys, ASTM STP 368, 1964, pp 28-40

32. Knittel, D. R. and Bronson, A., "Pitting Corrosion on Zirconium - A Review," Corrosion, Vol. 40 #1, January 1984, pp 9-14

33. Craig, D. B., Ed., Handbook of Corrosion Data, ASM, 1989

34. Riley, W. D. And Covino, B. S. Jr., "Effect of Ferric Ion on Corrosion Resistance of Zirconium in HCl-$AlCl_3$ Environment," BuMines RI 8610, February 1982

35. Manolescu, A. V., Mayer, P., and Simpson, C. J., "Effect of Lithium Hydroxide on Corrosion Rate of Zirconium 2.5 wt % Niobium in 340°C Water," Corrosion, Vol. 38 #1, January 1982 pp 23-31

36. McDonald, S. G., Sabol, G. P., and Sheppard, K. D., "Effect of Lithium Hydroxide on the Corrosion Behavior of Zircaloy-4," *Zirconium in the Nuclear Industry: Sixth International Symposium, ASTM STP 824*, Franklin, D. G. and Adamson, R. B. Eds., American Society for Testing Materials, 1984, pp. 519-530

37. Hillner, E., and Chirigos, J. N., "The Effect of Lithium Hydroxide and Related Solutions on the Corrosion Rate of Zircaloy in 680°F Water," WAPD-TM-307, Westinghouse Electric Corporation, August 1962

38. Cox, B., "Oxidation of Zirconium and its Alloys," Advances in Corrosion Science and Technology, Vol.5, Fontana, M. G. and Staehle, R. W., Eds., Plenum Press, 1976

39. Coriou, H., Grail, L., Meunier, J., Pelras, M. and Wilermoz, H., "Corrosion of Zircaloy in Various Alkaline Solutions at High Temperature," Journal of Nuclear Materials, Vol. 7 #3, 1962, pp 320-327

40. Pourbaix, M., *Atlas of Electrochemical Equilibria in Aqueous Solutions*, Pergamon Press, New York, N.Y., 1966, Section 8.2, p. 227

41. Little, B., and Wagner, P., "An Overview of Microbiologically Influenced Corrosion of Metals and Alloys Used in the Storage of Nuclear Wastes," Canadian Journal of Microbiology, Vol. 42, 1996, pp.367-374

42. McNeil, M., and Odom, A.,"Thermodynamic Prediction of Microbiologically Influenced Corrosion (MIC) by Sulfate-Reducing Bacteria (SRB)," *Microbiologically Influenced Corrosion Testing. ASTM STP 1232*, Kearns, J. R. and Little, B. J., Eds., American Society for Testing and Materials, Philadelphia, 1994, pp.173-179

43. Cox, B., "Rate Controlling Processes During The Pre-Transition Oxidation of Zirconium Alloys," Journal of Nuclear Materials, Vol. 31, 1969, pp 48-66

44. "Precipitate Stability in Zircaloy-4," EPRI Report NP-5591, January 1988

45. Yang, W.J.S., Tucker, R.P., Cheng, B., and Adamson R.B., "Precipitates in Zircaloy: Identification and The Effects of Irradiation and Thermal Treatment," Journal of Nuclear Materials, Vol. 138, 1986, pp 185-195

46. Griffiths, M., "A Review of Microstructure Evolution in Zirconium Alloys During Irradiation," Journal of Nuclear Materials, Vol. 159, 1988, pp 190-218

47. Garzarolli, F., Steinberg, E., and Weidinger H.G., "Microstructure and Corrosion Studies for Optimized PWR and BWR Zircaloy Cladding," *Zirconium in the Nuclear Industry: Eighth International Symposium, ASTM STP 1023*, Van Swam, L.F.P. and Eucken, C.M., Eds., American Society for Testing and Materials, Philadelphia, 1989, pp 202-212

48. "Corrosion of Zirconium Alloys in Nuclear Power Plants," IAEA-TECDOC-684, IAEA Vienna, January, 1993

49. Godlewski, J., "How the Tetragonal Zirconia is Stabilized in the Oxide Scale that is Formed on a Zirconium Alloy Corroded at 400°C in Steam," *Zirconium in the Nuclear Industry: Tenth International Symposium, ASTM STP 1245*, Garde, A.M., and Bradley, E.R., Eds., American Society for Testing and Materials, Philadelphia, 1994, pp. 663-686

50. Kido, T., "A Study on Enhanced Uniform Corrosion of Zircaloy-4 Cladding During High Burnup Operation in PWRs," *Proceedings, Sixth Symposium on Environmental Degradation of Materials in Nuclear Power Systems-Water Reactors*, Gold, R.E., and Simonen, E.P., Eds.,National Association of Corrosion Engineers, Houston, TX, 1993, pp 449-453

51. Kammenzind, B.F., Franklin, D.G., Peters, H.R., and Duffin, W.J., "Hydrogen Pickup and Redistribution in Alpha-Annealed Zircaloy-4," *Zirconium in the Nuclear Industry: Eleventh International Symposium, ASTM STP 1295*, Bradley, E.R., and Sabol, G.P., Eds., American Society for Testing and Materials, 1996, pp 338-369

52. Kearns, J.J., "Diffusion Coefficient of Hydrogen in Alpha Zirconium, Zircaloy-2 and Zircaloy-4," Journal of Nuclear Materials, Vol.43, 1972, pp 330-338

53. Ardell, A.J., and Sherby, O.D., "The Steady-State Creep of Polycrystalline Alpha Zirconium at Elevated Temperatures," Transactions of the Metallurgical Society of AIME, Vol.239, October 1967, p. 1547

54 Rosa, C. J., "Oxidation of Zirconium - A Critical Review of the Literature," Journal of Less Common Metals, Vol. 16, 1968, pp. 173-201

55. St. Jacques, R. G. and Angers, R., "Creep of CaO-Stabilized ZrO_2," Journal of the American Ceramic Society, Vol. 55, No. 11, 1972, pp. 571-574

56. Beie, H.-J., Mitwalsky, A., Garazarolli, F., Ruhmann, H., and Sell, H.-J., "Examinations of the Corrosion Mechanism of Zirconium Alloys," *Zirconium in the Nuclear Industry: Tenth International Symposium, ASTM STP 1245*, Garde, A.M., and Bradley, E.R., Eds., American
Society for Testing and Materials, Philadelphia, 1994, pp 615-643

57. Clarke, C. W. L., "The Safe Disposal of Nuclear Waste," Science and Technology Review, a publication of the Lawrence Livermore National Laboratory, March 1996, pp 6-16

58. Cheng, B.-C., Kruger, R.M., and Adamson, R.B., "Corrosion Behavior of Irradiated Zircaloy," *Zirconium in the Nuclear Industry: Tenth International Symposium, ASTM STP 1245*, Garde, A.M. and Bradley, E.R., Eds. American Society for Testing and Materials, Philadelphia, 1994, pp 400- 418

59. Boase, D.G., and Vandergraaf, T.T., "The Canadian Spent Fuel Storage Canister: Some Materials Aspects," Nuclear Technology, Vol. 32, January 1977, pp 60-71

60. Suzuki, M., and Kawasaki, S., "Oxidation of Zircaloy in Air," Journal of Nuclear Materials, Vol. 140, 1986, pp 32-43

61. Einziger, R.E., "Preliminary Spent LWR Fuel Oxidation Source Term Model," *High Level Radioactive Waste Management, Proceedings of the Fifth Annual International Conference, Las Vegas, Nevada, May 22-26, 1994* , American Nuclear Society, Inc., La Grange Park, Illinois, Vol.2, 1994, pp 554-559

62. Van Swam, L.P.F., and Shann, S.H., "The Corrosion of Zircaloy-4 Cladding in Pressurized Water Reactors,"*Zirconium in the Nuclear Industry: Ninth International Symposium, ASTM STP 1132*, Eucken, C.M., and Garde, A.M., Eds. American Society for Testing and Materials, Philadelphia, 1991, pp 758-781

63. "MATPRO: Version 10, A Handbook of Materials Properties for Use in the Analysis of Light Water Reactor Fuel Rod Behavior," TREE-NUREG-1180, 1978

64. Maguire, M., "The Pitting Susceptibility of Zirconium in Aqueous Cl^-, Br^-, and I^- Solutions," *Industrial Applications of Titanium and Zirconium: Third Conference, ASTM STP 830*, R.T. Webster and C.S. Young, Eds., American Society for Testing and Materials, Philadelphia, 1984, pp.177-189

Table 1: Comparison of Predictions From Eight Models for the Corrosion of Zircaloy after 10,000 Years at 180°C (356°F)

				ΔW	Thickness
Investigator [REF]	B	Q_1/R	K_1	mg/dm^2	mils
Hillner [11]	1.12E+08	-12529	1.10E-04	402	1.1
van der Linde [12]	2.30E+09	-14451	3.25E-05	119	0.3
Dyce [13]	6.53E+09	-15109	2.16E-05	79	0.2
Dalgaard [14]	1.84E+07	-11222	3.23E-04	1181	3.1
Billot [15]	1.13E+08	-12567	4.95E-05	181	0.5
Garzarolli [16]	1.18E+09	-13815	1.02E-04	374	1.0
Stehle [17]	2.21E+09	-14242	6.80E-05	248	0.7
Peters [18]	8.12E+08	-13512	9.12E-05	333	0.9

Table 2: Summary of Material and Test Conditions

Test No.	Test ID	Spec. No.'s*	Temp, °F	Material	Heat Treat
1	`5201	4/4	520	Zr-2	α
2	`5501	10/9	550	Zr-2	α
3	`5502	6/5	550	Zr-2	α
4	`5503	6/5	550	Zr-4	α
5	`6001	5/5	600	Zr-2	α
6	`6002	5/5	600	Zr-2	α
7	`6003	3/3	600	Zr-2	α
8	`6004	15/3	600	Zr-2	α
9	`6005	20/9	600	Zr-4	α
10	`6006	15/3	600	Zr-4	α
11	`6007	21/9	600	Zr-4	α
12	`6401	6/3	640	Zr-2	α
13	`6801	7/6	680	Zr-4	α
14	`6802	2/2	680	Zr-4	α
15	`6803	7/7	680	Zr-4	α
16	`6804	4/4	680	Zr-4	β
17	`6805	3/3	680	Zr-2	α
18	`6806	17/6	680	Zr-2	α
19	`6809	71/57	680	Zr-4	α
20	`68010	12/12	680	Zr-4	α
21	`68011	29/27	680	Zr-4	α
22	`68012	10/9	680	Zr-4	α & β

* The number to the left of the / shows the number of specimens at the start of the posttransition period and the number to the right of the / shows the number of specimens at the completion of the test.

Table 3: Summary of Dual Linear Posttransition Analyses

Test No.	Temp. Deg.F	1/T(K)	K(1)	K(2)	C(1)	time* tran.	W** tran.	time* max	W** max	ln[K(1)]	ln[K(2)]
1	520	1.84E-03	0.012	0.014	19.4			3000	60	-4.425	
2	550	1.78E-03	0.021	0.031	-3.4			9347	229	-3.863	
3	550	1.78E-03	0.028	0.024	-9.4			6381	163	-3.583	
4	550	1.78E-03	0.032	0.030	-2.5			6381	203	-3.442	
5	600	1.70E-03	0.064	0.103	-22.7	6874	419	10507	801	-2.745	-2.274
6	600	1.70E-03	0.077	0.110	-23.9	6461	473	10059	912	-2.565	-2.210
7	600	1.70E-03	0.085	0.107	-28.3	5855	472	8441	839	-2.461	-2.235
8	600	1.70E-03	0.092	0.200	-26.5	4251	366	7039	943	-2.382	-1.608
9	600	1.70E-03	0.075	0.122	-13.6	4320	310	7039	674	-2.592	-2.102
10	600	1.70E-03	0.080	0.103	-17.9	4522	342	7039	600	-2.531	-2.269
11	600	1.70E-03	0.078	0.135	-15.4	4498	334	7039	725	-2.555	-2.004
12	640	1.64E-03	0.200	0.271	-41.8	3134	584	6392	1665	-1.611	-1.307
13	680	1.58E-03	0.364	0.487	-22.4	679	225	1568	688	-1.011	-0.719
14	680	1.58E-03	0.356	0.488	-18.8	720	237	1554	651	-1.034	-0.717
15	680	1.58E-03	0.362	0.496	-18.2	672	225	1560	722	-1.017	-0.702
16	680	1.58E-03	0.329	0.441	- 7.7	493	154	1568	663	-1.113	-0.819
17	680	1.58E-03	0.438	0.715	-38.0	887	351	1568	941	-0.825	-0.336
18	680	1.58E-03	0.255	0.395	-7.8	869	214	1848	647	-1.365	-0.928
19	680	1.58E-03	0.376	0.444	-24.2	1184	421	2854	1265	-0.977	-0.813
20	680	1.58E-03	0.354	0.412	-20.4	1292	438	2854	1169	-1.037	-0.887
21	680	1.58E-03	0.339	0.440	-18.4	1256	407	2854	1246	-1.082	-0.821
22	680	1.58E-03	0.407	0.556	-4.1	1009	406	2730	1485	-0.899	-0.587

* Time, in days
**Weight Gain, in mg/dm^2
Transition time and transition weight gain, in this context, are between stage-1 and stage-2 linear kinetics

Table 4: Comparison of Predictions From Nine Models for the Corrosion of Zircaloy after 10,000 Years at 180°C (356°F)

				ΔW	Thickness
Investigator [REF]	B	Q_l/R	K_l	mg/dm^2	mils
Hillner [11]	1.12E+08	-12529	1.10E-04	402	1.1
van der Linde [12]	2.30E+09	-14451	3.25E-05	119	0.3
Dyce [13]	6.53E+09	-15109	2.16E-05	79	0.2
Dalgaard [14]	1.84E+07	-11222	3.23E-04	1181	3.1
Billot [15]	1.13E+08	-12567	4.95E-05	181	0.5
Garzarolli [16]	1.18E+09	-13815	1.02E-04	374	1.0
Stehle [17]	2.21E+09	-14242	6.80E-05	248	0.7
Peters [18]	8.12E+08	-13512	9.12E-05	333	0.9
This Work, Equ. [6]	2.46E+08	-12877	1.12E-04	410	1.1
This Work, Equ. [7]	3.47E+07	-11452	3.67E-04	1341	3.5

As with Table 1, all of the numbers in Table 4 have been rounded.

Table 5: Composition of J-13 Well Water

Chemical Species	Concentration (mg/L or ppm)
Na^{+}	46
Si^{4+}	29
Ca^{2+}	13
K^{+}	5
Mg^{2+}	2
B^{3+}	0.13
Li^{+}	0.05
HCO_3^{-}	130
$SO4^{=}$	18
$NO3^{-}$	8
Cl^{-}	7.1
F^{-}	2.2
pH = 7.4	

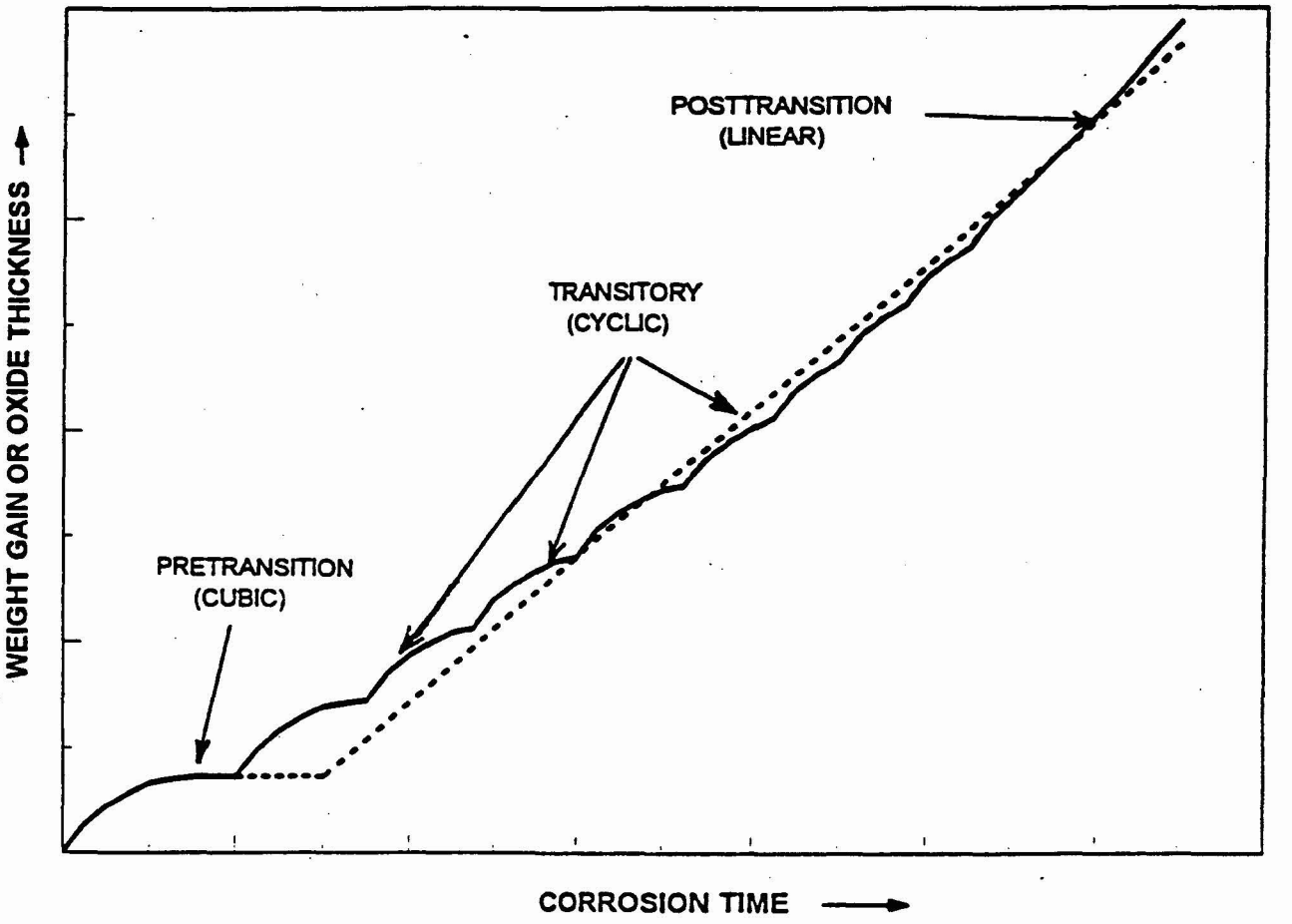

Figure 1: Schematic Drawing Showing the Three Zircaloy Corrosion Regions: Pretransition, Transitory, and Posttransition. The Dashed Lines Indicate that Early Models Recognized Only the Pretransition and Posttransition Kinetic Regimes.

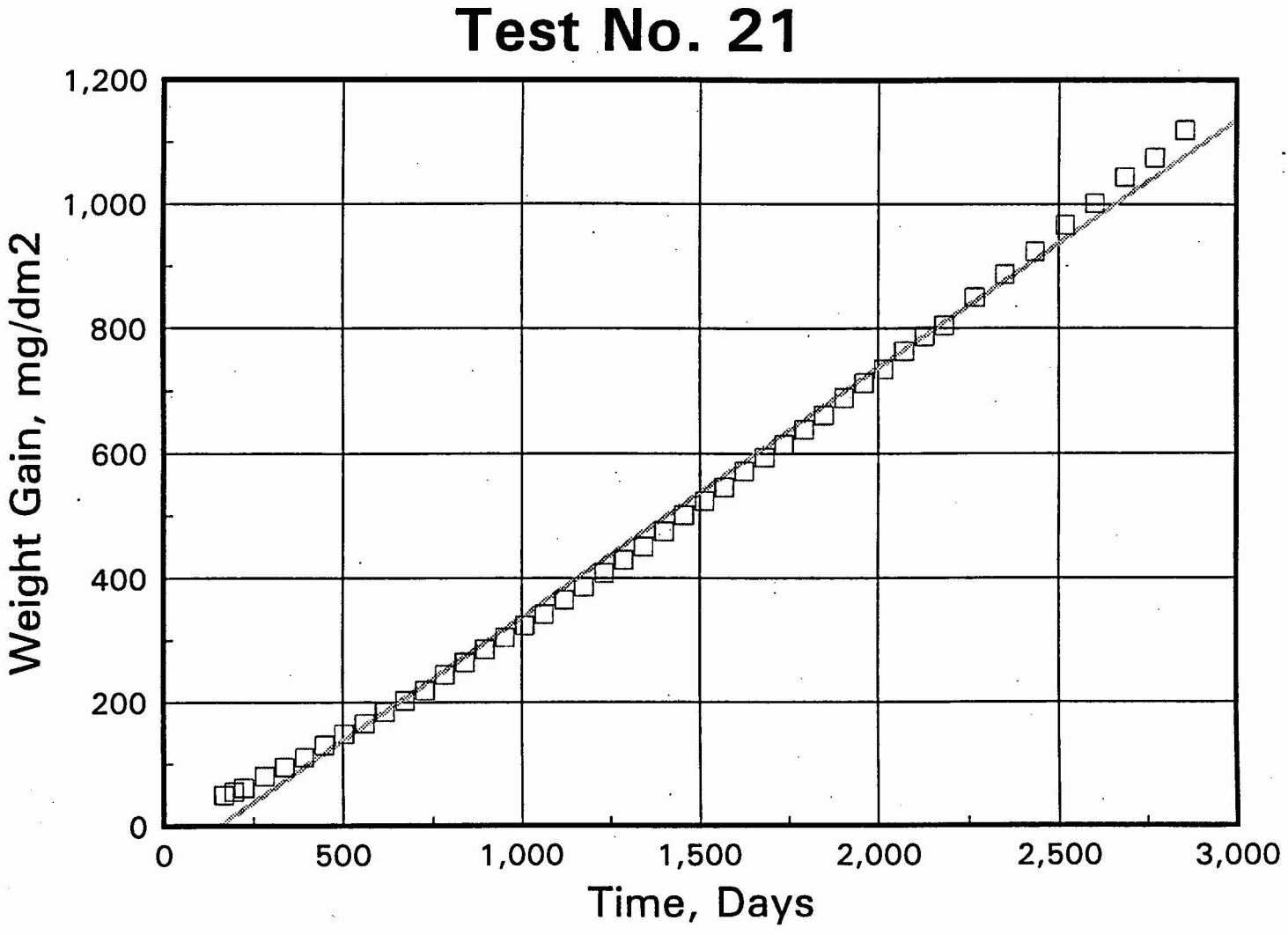

Figure 2A: Corrosion of Zircaloy-4 in 680°F (360°C) Water - Test No. 21. Data Show Curvature About a Single Least-Squares Straight Line.

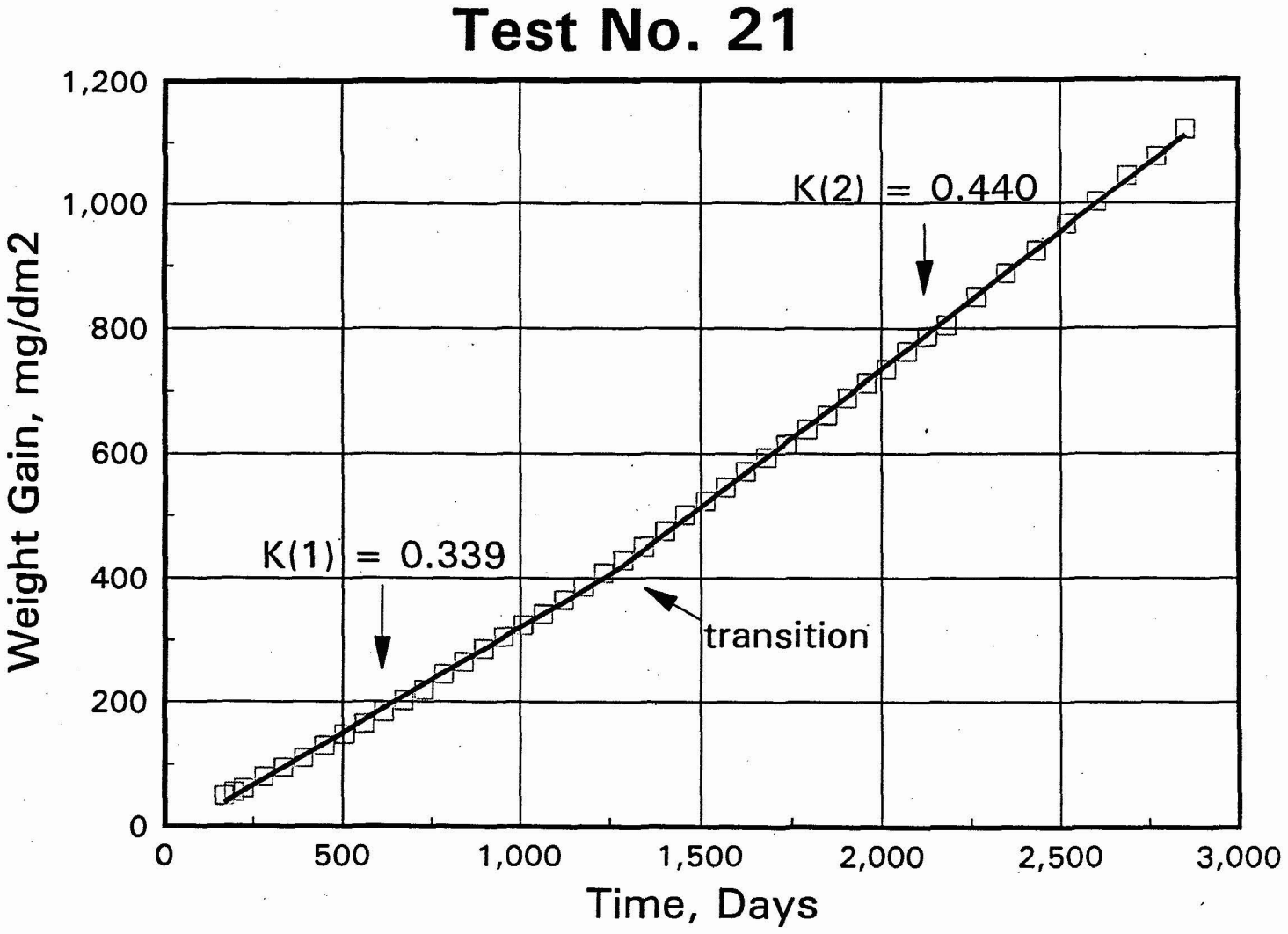

Figure 2B: Same Data as in Figure 2A, Replotted to Show that a Dual Linear Relationship is a Better Representation of the Weight Gain/Time Measurements.

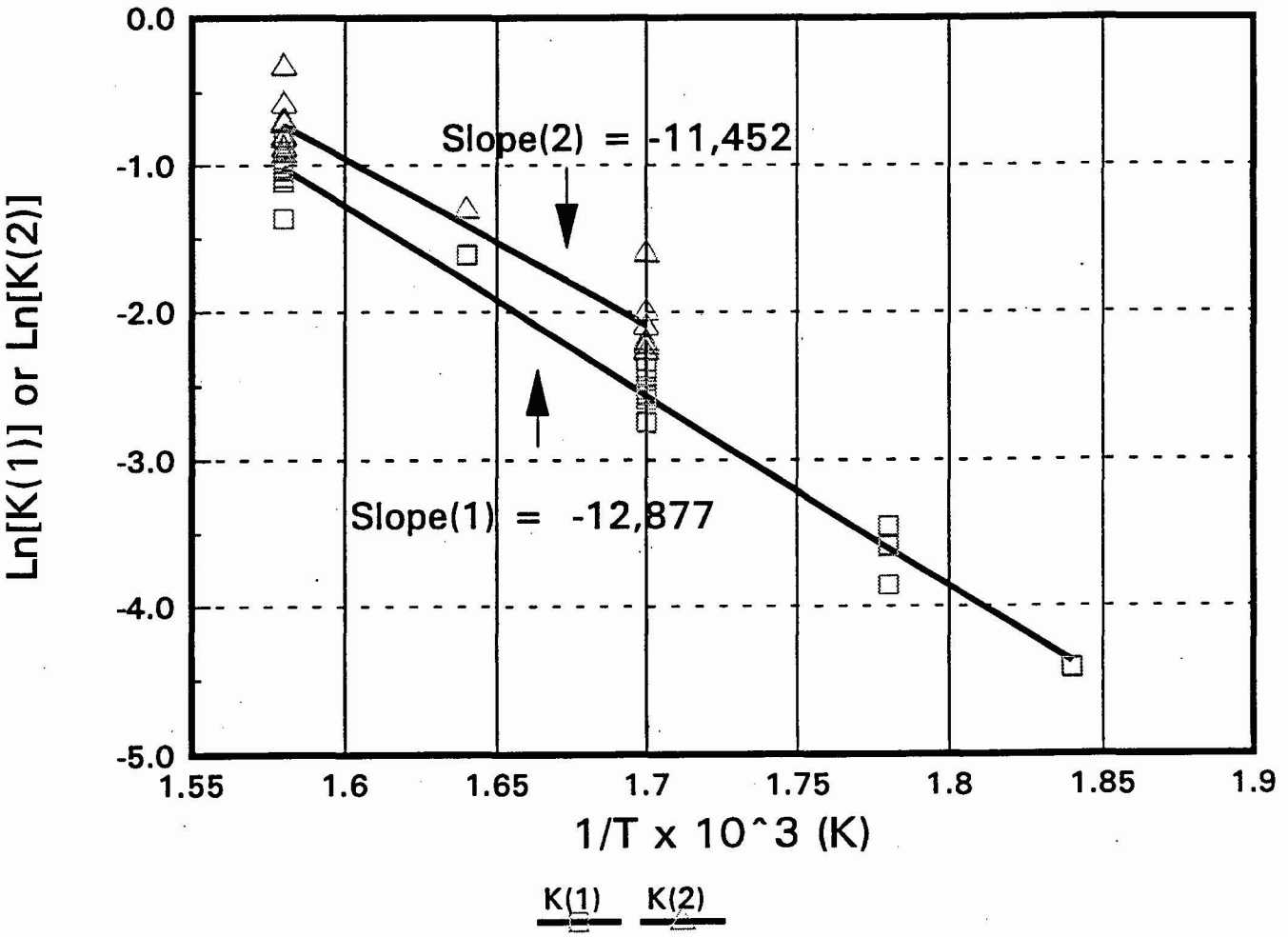

Figure 3: Stage-One and Stage-Two Linear Rate Constants as a Function of the Inverse Absolute Temperature.

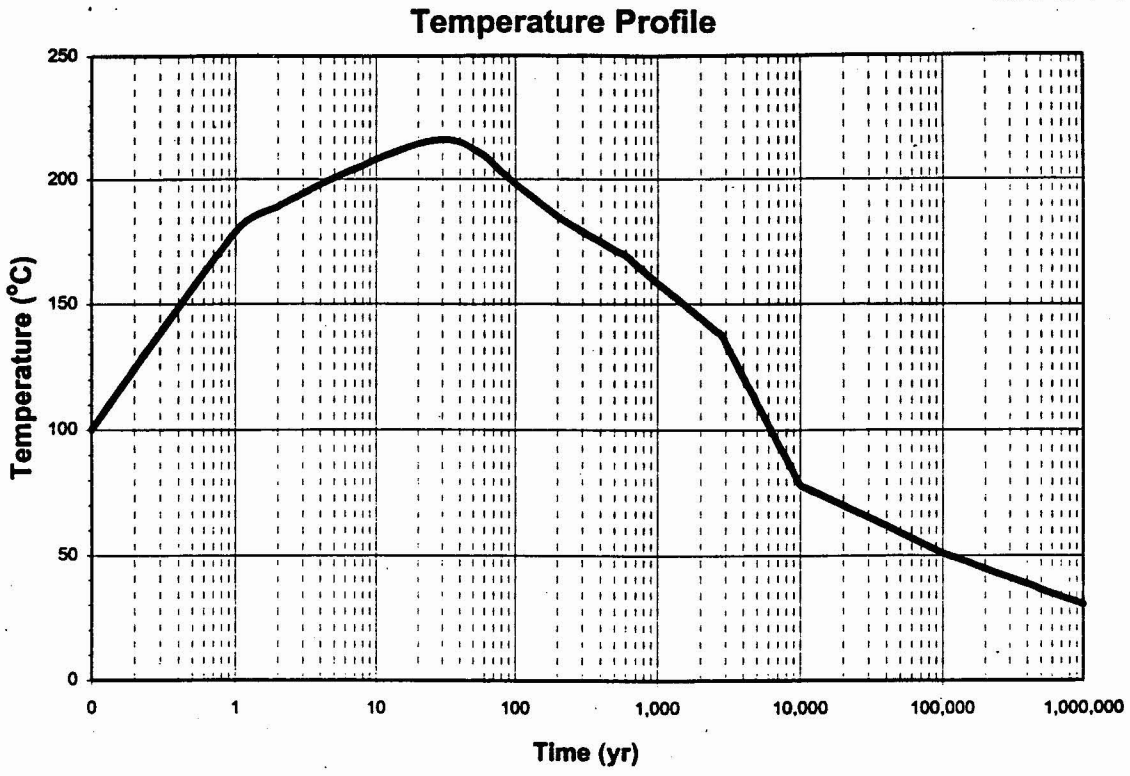

Figure 4A: Anticipated Decay Heat Curve for Expended Naval Fuel in Yucca Mountain Repository.

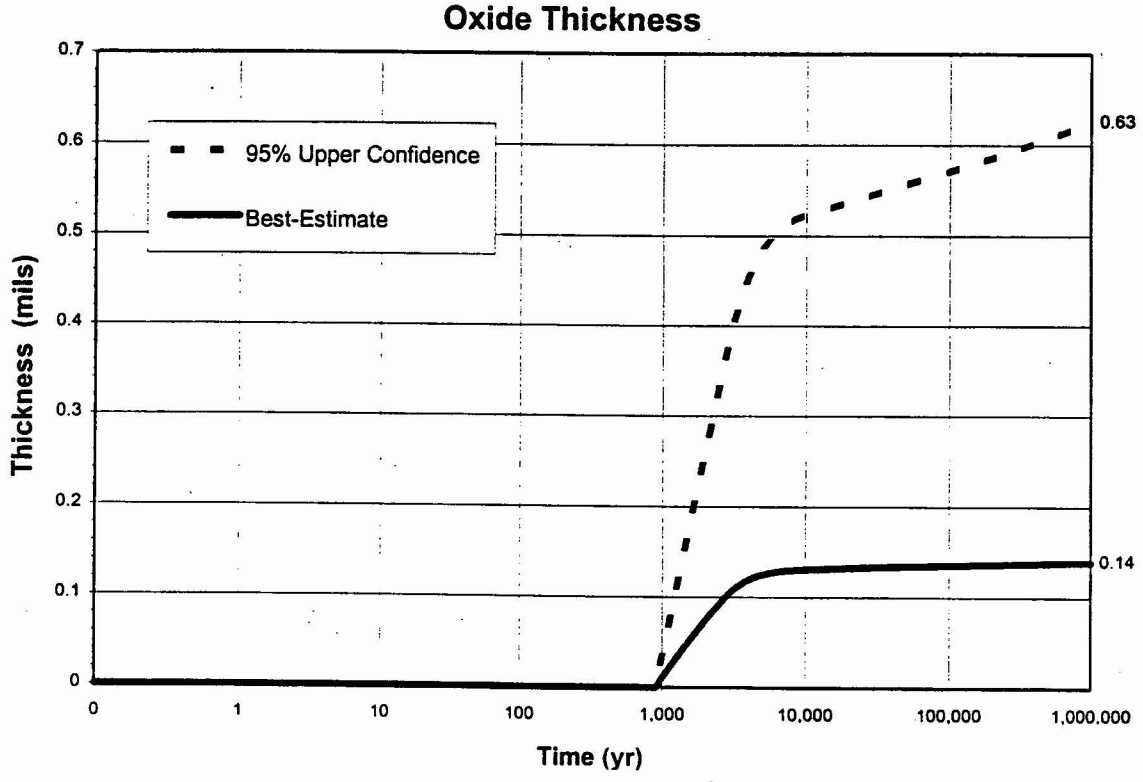

Figure 4B: Estimated Additional Corrosion on Zircaloy Cladding During Yucca Mountain Disposal. Based on Temperatures from Figure 4A and Use of Equation [7].

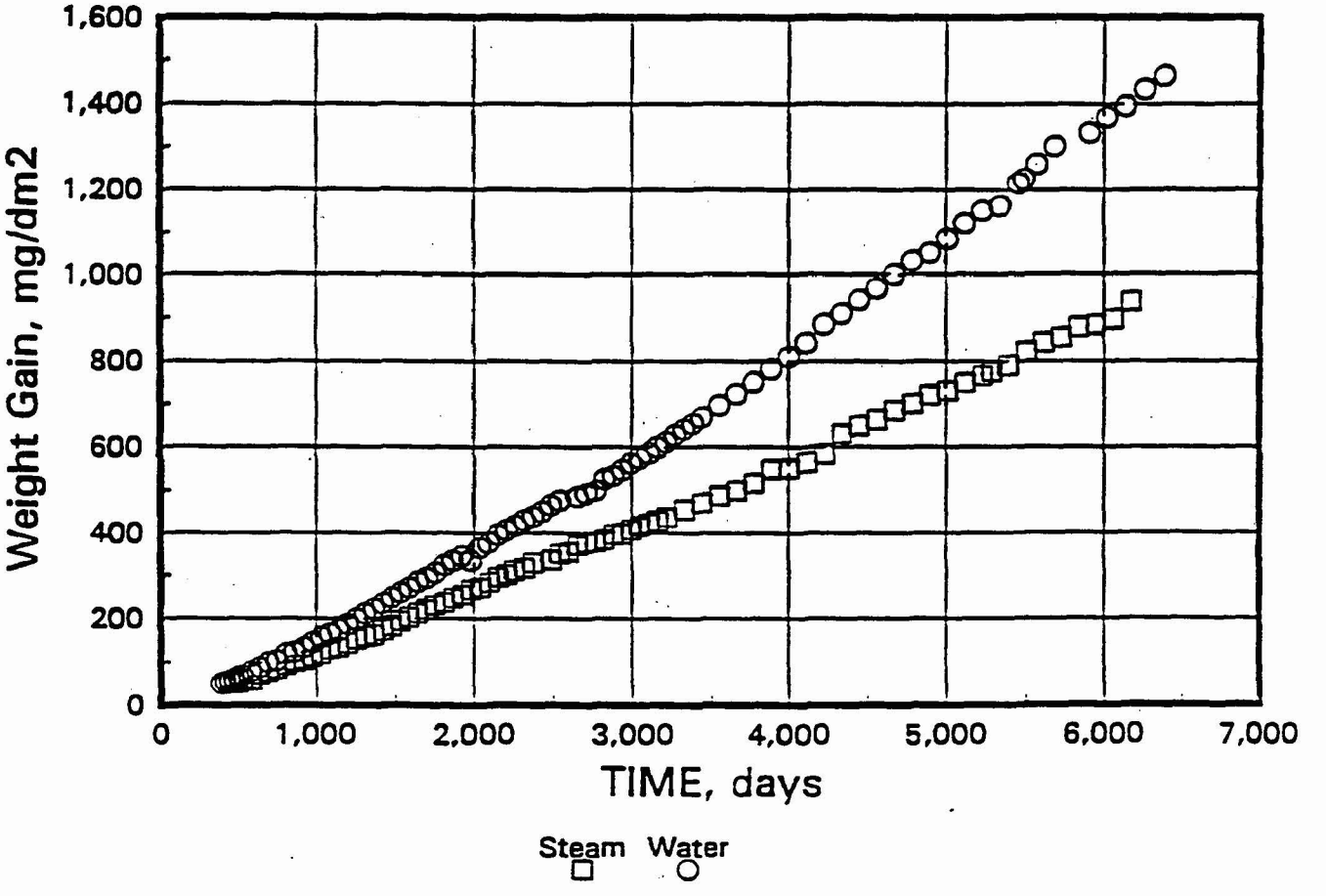

Figure 5: Corrosion of Alpha-Annealed Zircaloy-2 at 640°F (338°C) Steam vs. Water Exposure.

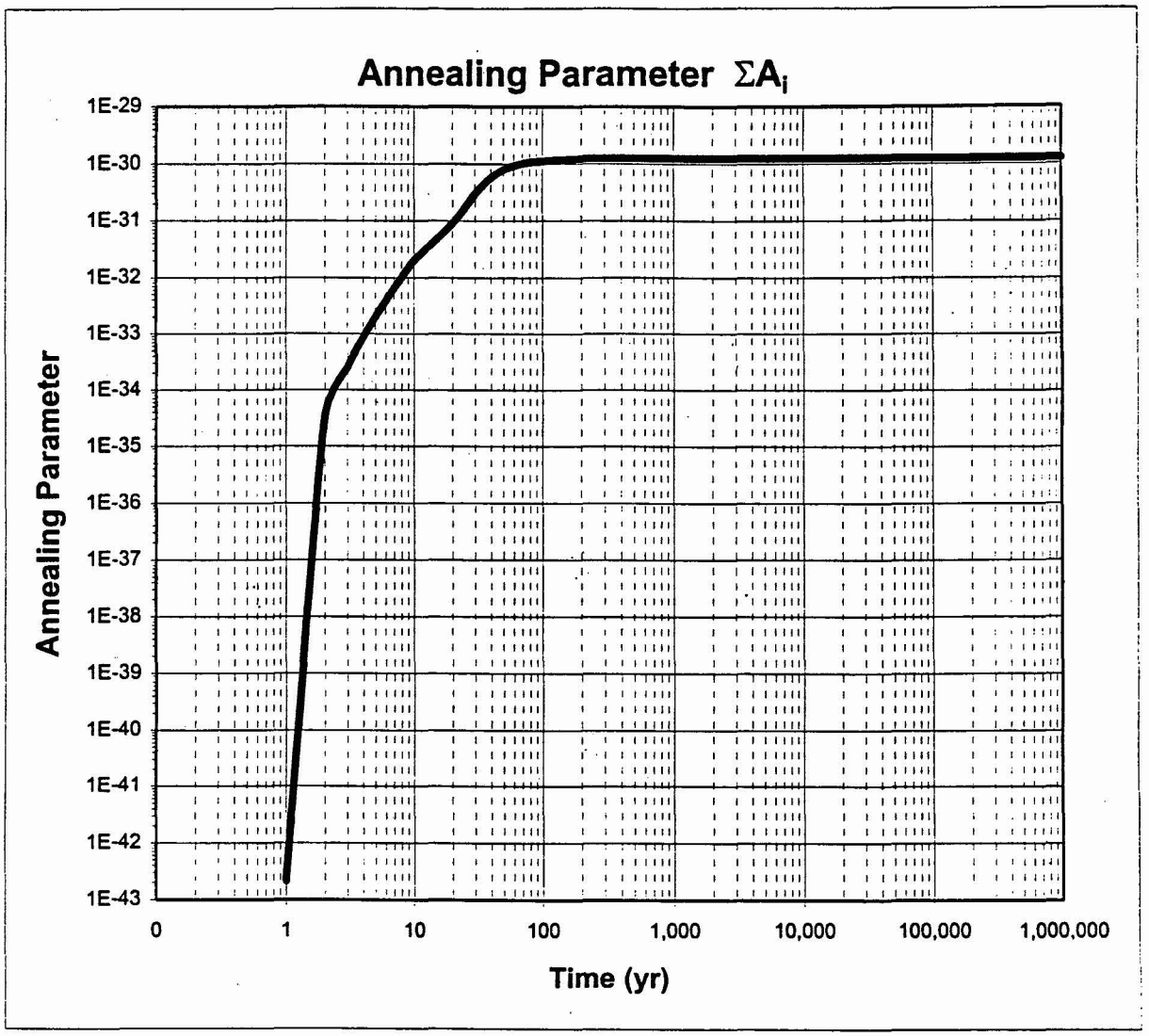

Figure 6: Cumulative Annealing Parameter (ΣA_i) Based Upon Anticipated Repository Temperature Profile of Figure 4A.

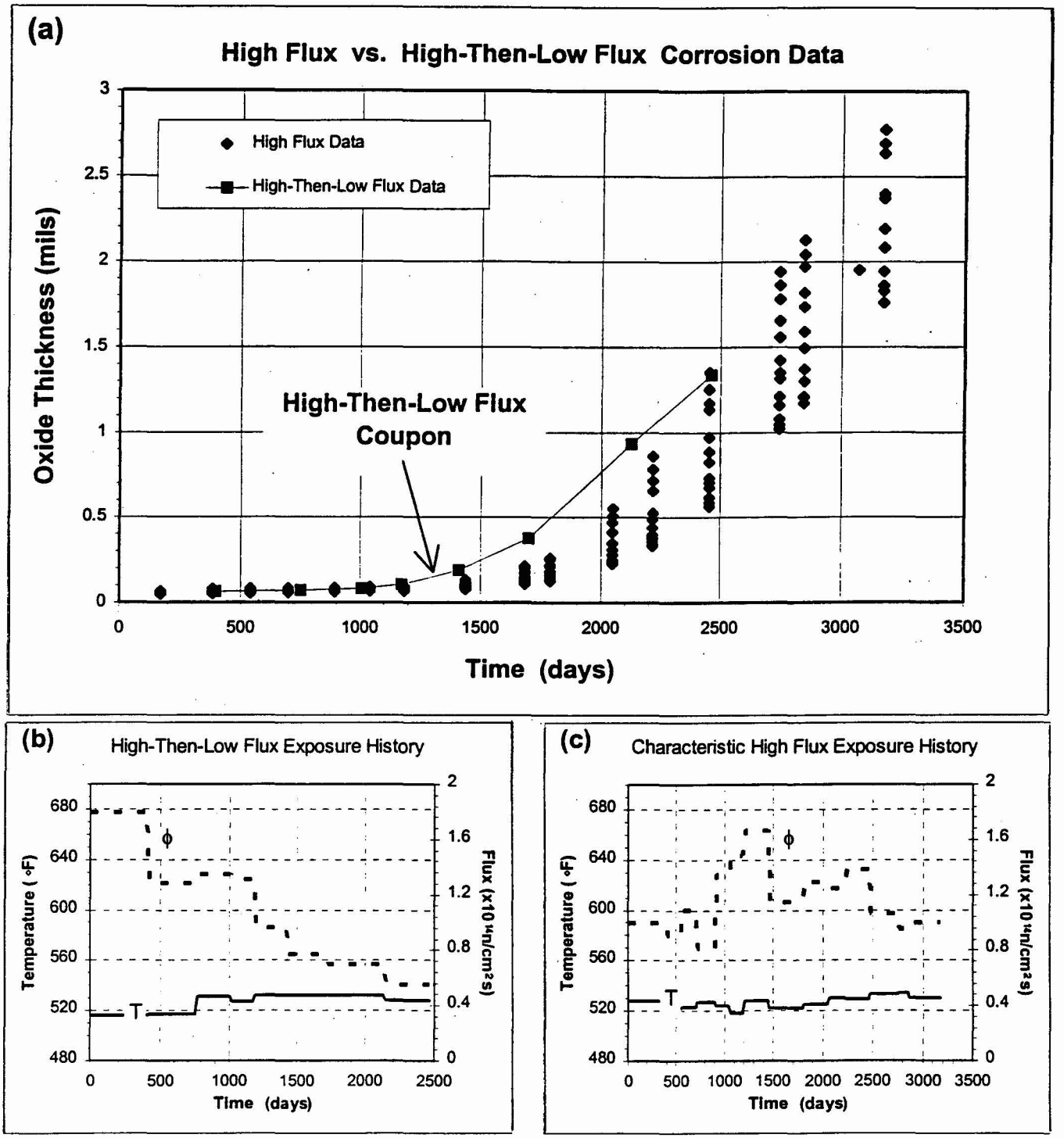

Figure 7: Effect of Shift in Flux on Subsequent In-Pile Corrosion Rate.

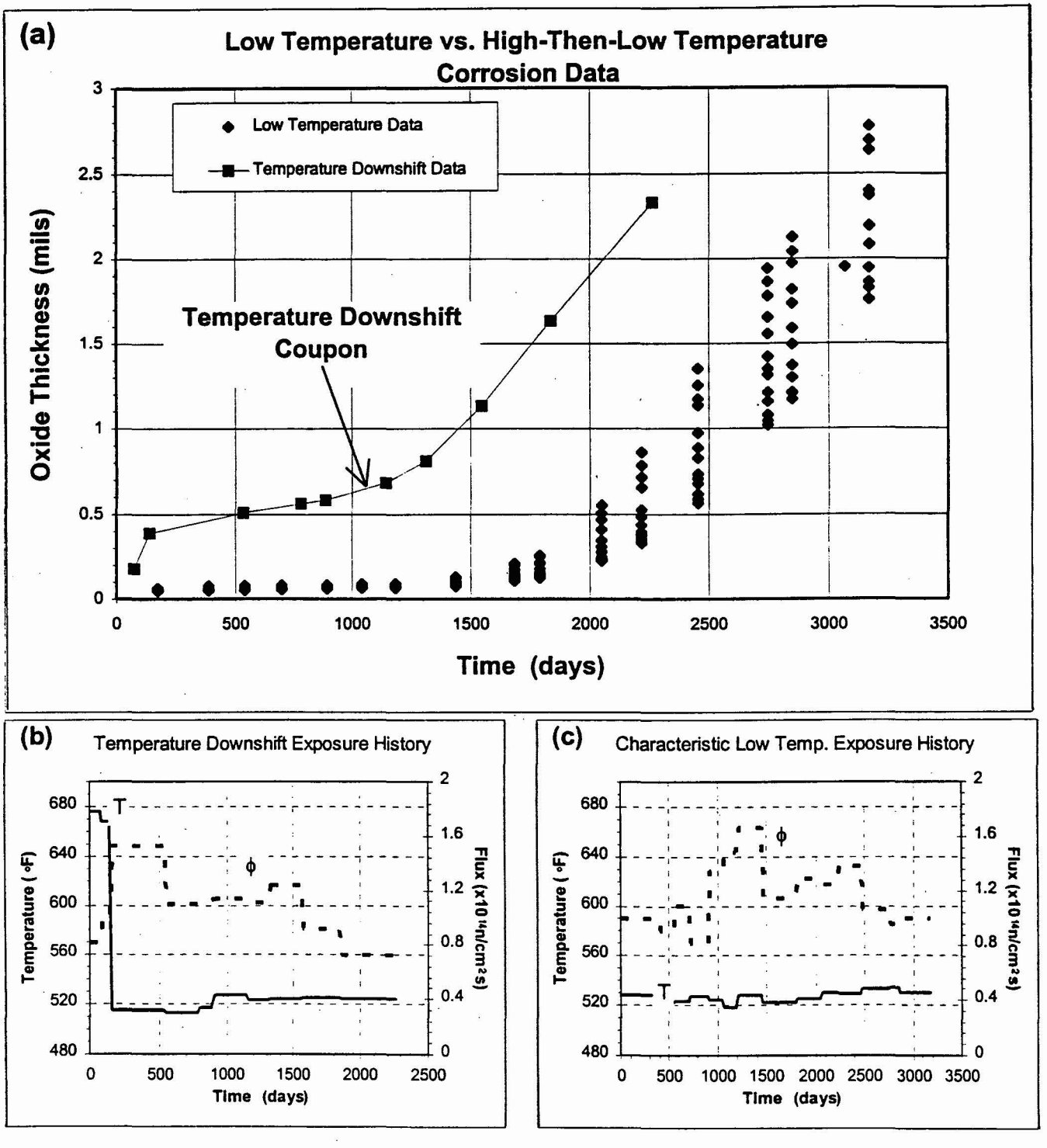

Figure 8: Effect of Shifts in Temperature and Flux on Subsequent In-Pile Corrosion Rate.

STATISTICAL ANALYSIS OF AUTOCLAVE CORROSION DATA

WALTER A. MEYER

Statistical Analysis

This section documents the analysis methodologies used to arrive at the conclusions presented in the report. The outline is in four sections:

1. Handling the raw data and identifying outliers.
2. Fitting the curves with a multiphase model.
3. The database of results and Arrhenius behavior.
4. Uncertainty of the best fit line.

1. Handling the raw data and identifying outliers

The data from twenty-two separate autoclave tests were recorded in a spreadsheet. Most runs were comprised of only a single heat of material. Since the data spanned many years and some of it was recorded and entered into a computer manually, the first procedure used to analyze the data was to check for outliers. Each run consisted of three to fifty-seven individual specimens tested over a few thousand days to up to ten thousand days. To detect changes in the variability, the standard deviation of the specimens was computed and plotted for each time it was recorded. A sample plot is shown in Figure A.1 for one run at 600 °F. As the figure shows, the variability among the specimens tends to increase as the weight gain increases. This is typical behavior of a gage that has error proportional to range or scale. The figure also indicates two possible anomalies in that run. Each anomaly was investigated. For the circled point in the figure, it was found that one of the specimens had an unusually low value recorded at that temperature which caused the standard deviation of the specimens to roughly triple. It was also observed that the recorded weight gain was inconsistent with both the value immediately prior to, and immediately following, this exposure time. Since that data point was obviously bad it was removed. Without that point, the standard deviation came back into normal range. The other point in the figure that seemed too high was investigated and no highly unusual values were found. Thus, this point was retained in the database. No further data were removed from this run.

For the rest of the runs, this charting technique identified potentially bad data, which were removed for various reasons, e.g., digits reversed, a digit left out, data for two temperatures reversed, etc. When anomalies were found the only two actions taken were to leave the data point in the database or to remove the data point from the database. Thirteen bad data points, out of a total of 11,062 data, were found and removed.

2. Fitting the curves with a multiphase model

With the identifiable outliers removed, the average specimen weight was computed for each of the twenty-two runs. There were from two to twenty-one specimens in this average. For most runs, more specimens started than finished the test. Although all of the data were used to compute the average weight gain for the run, the recorded number of specimens for a test represented only those specimens that lasted through the entire duration of the test.

The average weight gain versus time data was then put into the SOLO statistical software package. This package found that a two-phase linear model produced the simplest fit to the data. The multiphase linear-linear model is made up of two linear equations, each active over a different time range. The software automatically calculates the transition point from one phase to another, and no smoothing was used in calculating the transition point. A sample of the output

from the multiphase curve fit routine (for the same run at 600 °F used to make Figure A.1) is shown in Table A.1 and Figure A.2. All of these data were obtained from test #5 in the text.

Of interest in Table A.1 is the summary of parameters in the common model at the bottom of the figure. It shows the two linear models with intercepts C(1) and C(2) and slopes K(1) and K(2) and the transition point α. The transition point α is shown in days. Figure A.2 graphically shows the data along with the two-phased linear model. The eye immediately focuses on the lack of fit in the low weight gain portion of the curve. This is due to a different set of kinetics early in the corrosion process. The net effect of including this early weight gain data in the model is to bias the slope for the first linear phase and a smaller bias in the transition point. The effect is quite small, however. For example, when the data is restricted to weight gains of greater than 100, the slope changes from K(1) = 0.064 (shown in Table A.1 as 6.4224E-02) to K(1) = 0.068 and α changes from 6,874 days to 7,468 days.

3. The database of results and Arrhenius behavior

For each of the twenty-two runs, the five parameters (C(1), K(1), α, C(2), K(2)) for the two-phase linear models were recorded into a summary database. The values for K(1) and K(2) are reproduced in Table A.2. Also included in the table are the temperatures, the natural logs of the slopes and the inverse of the absolute temperature. From this data two linear models were fit. The fit of interest was the natural log of the slope versus the inverse of the absolute temperature. Materials theory suggests that these fits should be straight lines so simple linear regression was used to fit the data. (Note: A weighted least squares model, where the weights were the number of specimens completing each run, was also analyzed. The results were less conservative than those obtained with simple linear regression. The weighted model was subsequently abandoned in favor of the simple dual linear-regression model.)

A separate line was fit for each phase of the weight gain curves. Since no transition to a higher slope was observed for temperatures below 600°F, only the 600, 640, and 680°F data were used to fit the line through the natural logarithms of the phase-two slopes (K(2)'s). A plot of the data and the best fit lines is shown in Figure A.3 (and Figure 3 in the text).

4. Uncertainties of the best line fit

Since simple linear regression was used to fit the data, a standard 95% confidence interval for the mean ln(Q/R) at a chosen point, x*, (where x* is in units of 1/T) is:

$$a + bx^* \pm t_{n-2}\, S_e\, [(1/n) + (x^* - x)^2/S_{xx}]^{1/2}$$

The values for the parameters for line 2 can be found in Table A.2 and used with any x*:

a = 17.36226
b = -11,451.6
n = 18
x = 0.00163
t_{n-2} = 2.12
S_e = 0.1954
S_{xx} = 5.87E-8
This uncertainty for the mean ln(Q/R) is applicable to temperatures within the 600°F to 680°F band.

Table A.1

Estimation Summary Report

Model: Y = A+BX+(X-D) * C * SGN(X-D)
Y: Weight Gain X: Time

Term	Coefficient Estimate	Std. Error	T-Value Prob	(|t| >T)	R-Squared
A	-155.4187	6.60	-23.5	0.0000	0.9984
B	8.3537531D-02	7.94E-04	105.1	0.0000	
C	1.931366D-02	7.94E-04	24.3	0.0000	
D	6874.11	91.45	75.2	0.0000	

Source	df	Sum-Sqr	Mean Square	SQR(M.S.)	F-Ratio	Prob (f>F)
Model	3	3739838	1246613	1116.518	22253.7	0.0000
Error	109	6105.982	56.01819	7.48453		
Total	112	3745944	33445.93	182.8823		

Parameters in Common Model

Y = C(1) + K(1) (X) $X \leq \alpha$

Y = C(2) + K(2) (X) $X > \alpha$

C(1) = -22.65 C(2) = -288.1

K(1) = 6.422E-02 K(2) = .1028

α = 6874

where α = transition time, days

Table A.2 Slope Parameters and Regression Fits

Test No.	Temp (F)	K(1)	K(2)	lnK(1)	lnK(2)	1/T(K)
1	520	0.0120	0.0142	-4.4251	-4.2556	1.84E-03
2	550	0.0211	0.0313	-3.8590	-3.4645	1.78E-03
3	550	0.0276	0.0236	-3.5887	-3.7456	1.78E-03
4	550	0.0317	0.0296	-3.4502	-3.5189	1.78E-03
5	600	0.0642	0.1029	-2.7454	-2.2745	1.70E-03
6	600	0.0769	0.1097	-2.5652	-2.2098	1.70E-03
7	600	0.0854	0.1070	-2.4609	-2.2347	1.70E-03
8	600	0.0923	0.2002	-2.3822	-1.6083	1.70E-03
9	600	0.0749	0.1222	-2.5917	-2.1017	1.70E-03
10	600	0.0796	0.1034	-2.5306	-2.2696	1.70E-03
11	600	0.0777	0.1348	-2.5553	-2.0043	1.70E-03
12	640	0.1997	0.2706	-1.6110	-1.3073	1.64E-03
13	680	0.3640	0.4875	-1.0106	-0.7185	1.58E-03
14	680	0.3557	0.4881	-1.0336	-0.7172	1.58E-03
15	680	0.3616	0.4955	-1.0173	-0.7022	1.58E-03
16	680	0.3285	0.4407	-1.1131	-0.8195	1.58E-03
17	680	0.4382	0.7148	-0.8251	-0.3357	1.58E-03
18	680	0.2553	0.3953	-1.3651	-0.9280	1.58E-03
19	680	0.3763	0.4436	-0.9774	-0.8128	1.58E-03
20	680	0.3544	0.4120	-1.0373	-0.8867	1.58E-03
21	680	0.3391	0.4399	-1.0815	-0.8213	1.58E-03
22	680	0.4071	0.5558	-0.8988	-0.5873	1.58E-03

Regression Output:	Line 1 (Stage-one Linear)
Constant	19.3224
Std Err of Y Est	0.1377
R Squared	0.9852
No. of Observations	22
Degrees of Freedom	20
X Coefficient(s)	-12876.96
Std Err of Coef.	352.36
Sxx	1.53E-07
95_U	-12140.5
95_L	-13613.4

Regression Output:	Line 2 (Stage-two Linear)
Constant	17.3623
Std Err of Y Est	0.1954
R Squared	0.9264
No. of Observations	18
Degrees of Freedom	16
X Coefficient(s)	-11451.63
Std Err of Coef.	806.74
Sxx	5.87E-06
95_U	-9741.36
95_L	-13161.9

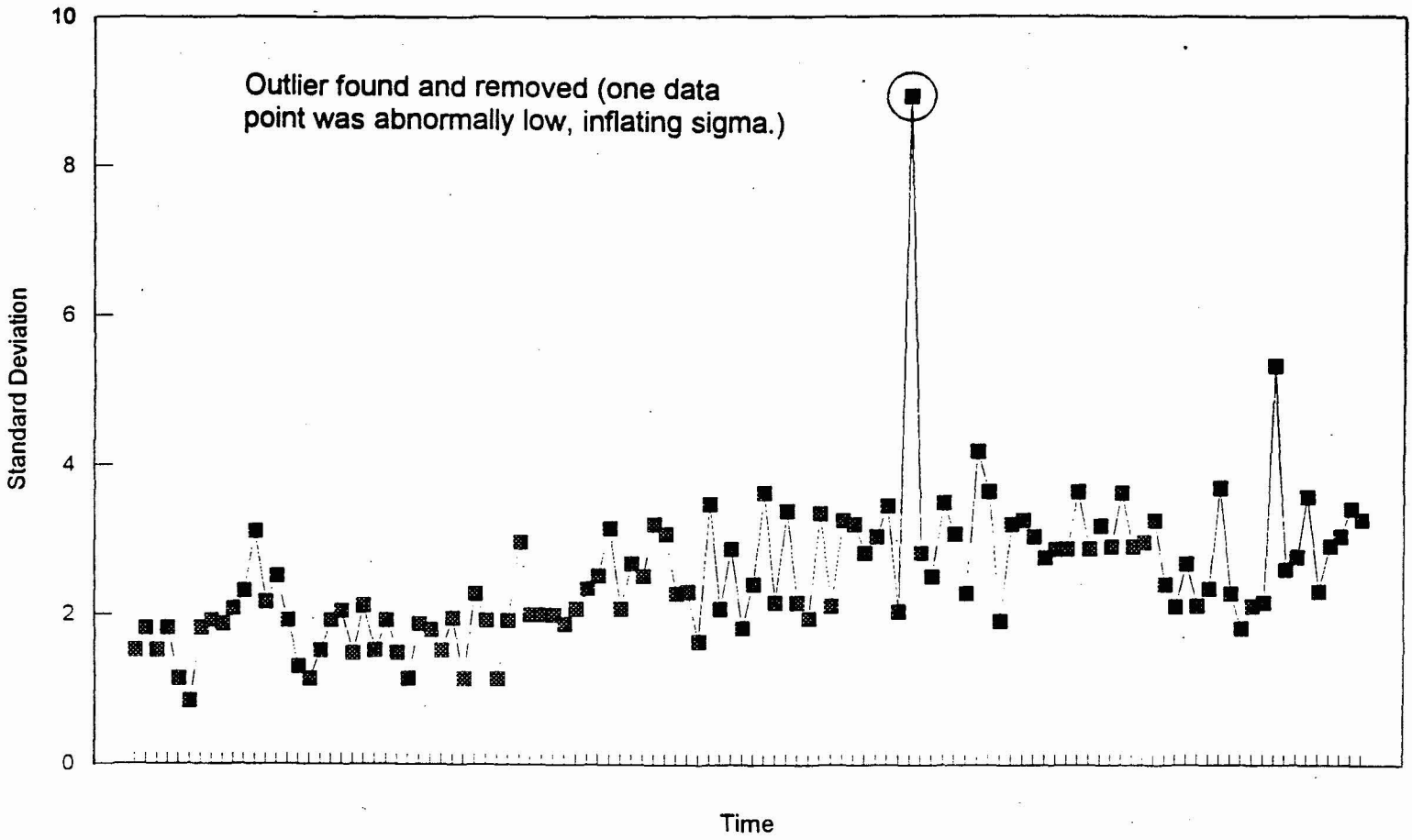

Figure A.1: Plot of Standard Deviation as a Function of Test Time, which was Used to Find Outlier Data in the Database.

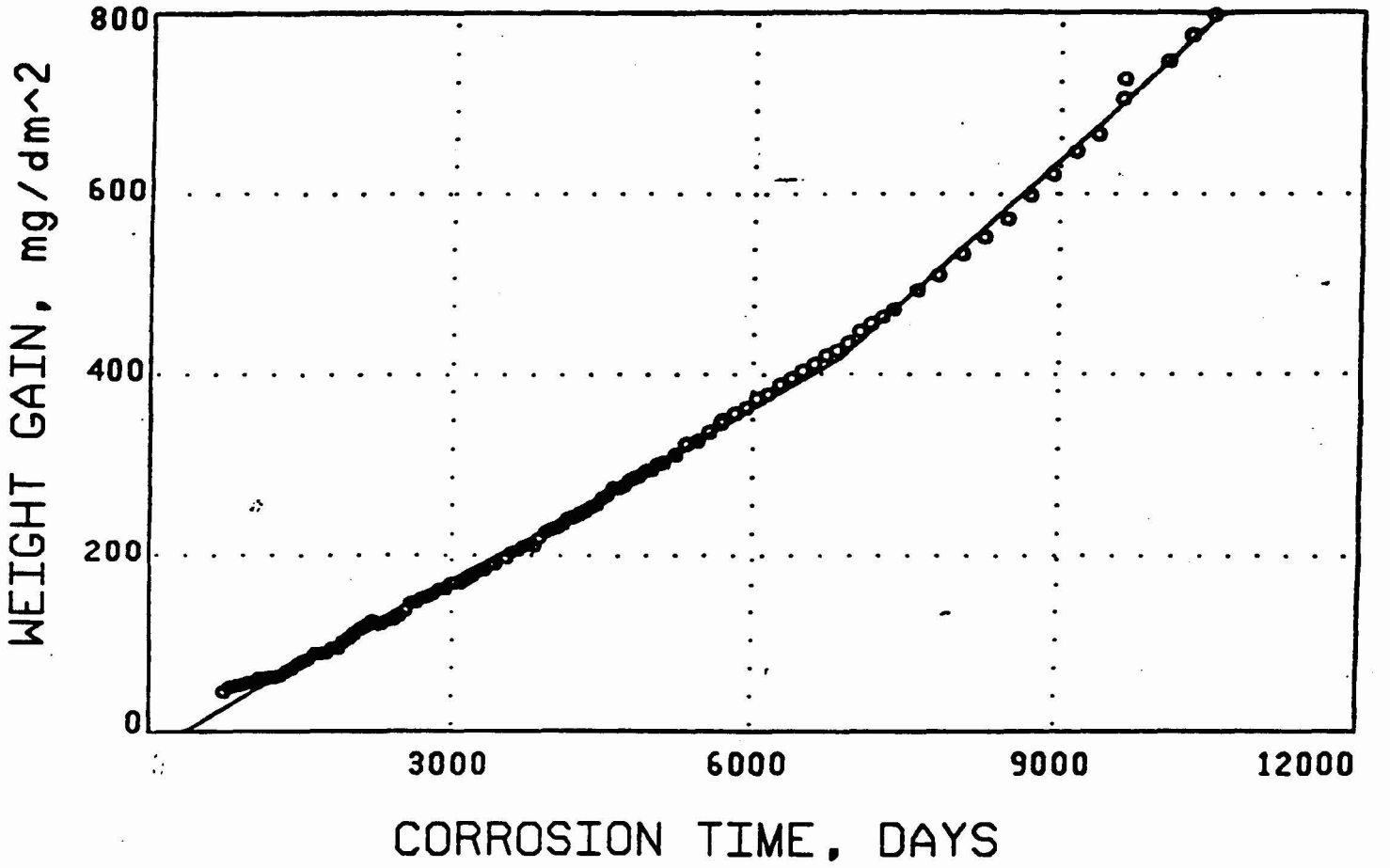

Figure A.2: Weight Gain as a Function of Test Time Compared to Statistically Fit Curve for a Typical Set of Data.

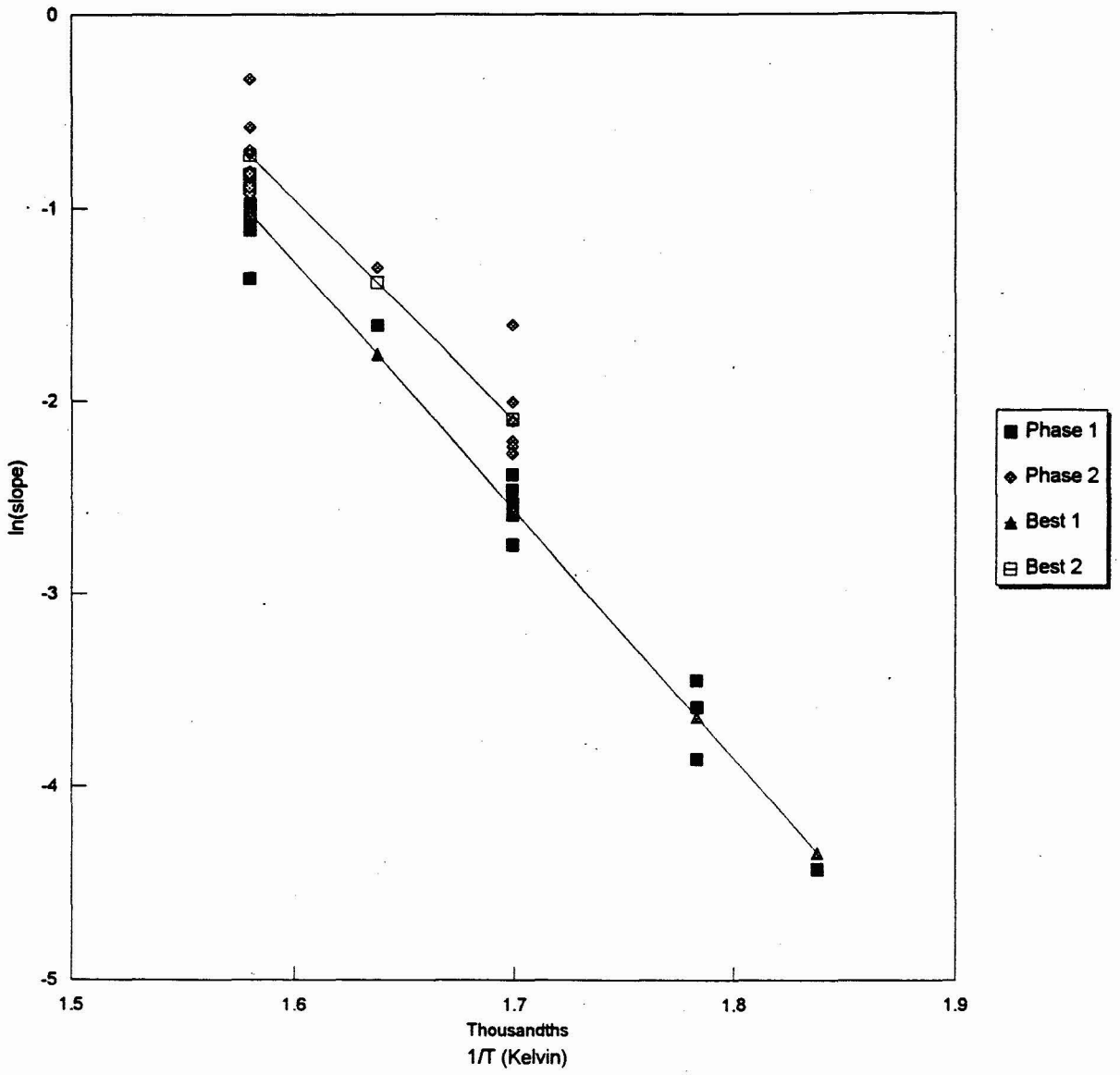

Figure A.3: Corrosion Weight-Gain Rates Versus Reciprocal Temperature, Which Reflects the Statistical Analysis to Determine the Thermal Activation Energy, Q.